AD-A074 340 ROCKWELL INTERNATIONAL THOUSAND OAKS CA SCIENCE CENTER F/G 13/8
FUNDAMENTALS OF PLASMA ARC WELDING.(U)
AUG 79 C B SHAW
UNCLASSIFIED SC5031.8FR N00014-75-C-0789
NL

1 OF 2
AD
A074340

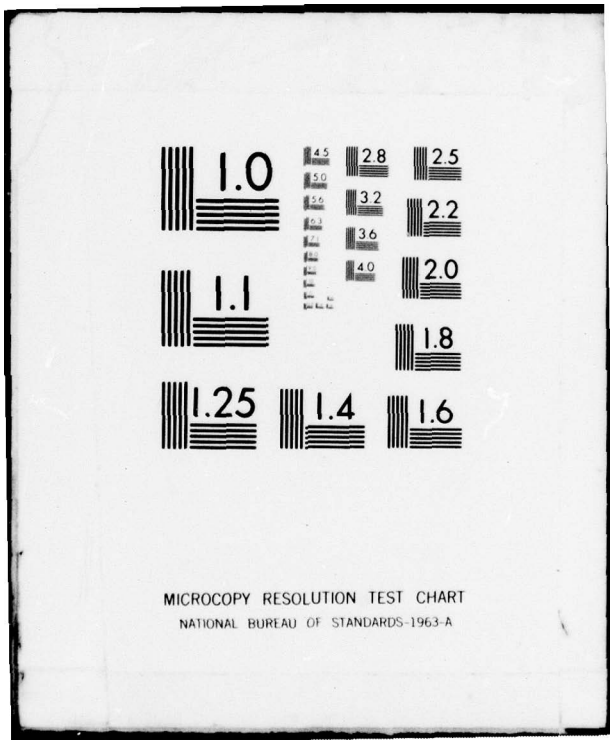
1.0
1.1
1.25
1.4
1.6
1.8
2.0
2.2
2.5
2.8
3.2
3.6
4.0
4.5
5.0
5.6
6.3
MICROCOPY RESOLUTION TEST CHART
NATIONAL BUREAU OF STANDARDS-1963-A

5

SC5031.8FR

FUNDAMENTALS OF PLASMA ARC WELDING

Final Report

Contract No. N00014-75-C-0789

Project No. 471

Prepared for

Office of Naval Research
Department of the Navy
800 North Quincy Street
Arlington, Virginia 22217

by

C.B. Shaw, Jr.

August 1979

Research sponsored by the Office of Naval Research under Contract No. N00014-75-C-0789 (Project No. 471).

Rockwell International
Science Center

UNCLASSIFIED

SECURITY CLASSIFICATION OF THIS PAGE (When Data Entered)

REPORT DOCUMENTATION PAGE	READ INSTRUCTIONS BEFORE COMPLETING FORM
1. REPORT NUMBER: (9) Final rept. 1 apr 75 – 30 Sep 78 (2) GOVT ACCESSION NO.	3. RECIPIENT'S CATALOG NUMBER
4. TITLE (and Subtitle): (6) FUNDAMENTALS OF PLASMA ARC WELDING	5. TYPE OF REPORT & PERIOD COVERED: Final Report 04/01/75 through 09/30/78
	6. PERFORMING ORG. REPORT NUMBER: (14) SC5031.8FR
7. AUTHOR(s): (10) C.B. Shaw, Jr.	8. CONTRACT OR GRANT NUMBER(s): (15) N00014-75-C-0789
9. PERFORMING ORGANIZATION NAME AND ADDRESS: Rockwell International Science Center, 1049 Camino Dos Rios, Thousand Oaks, California 91360	10. PROGRAM ELEMENT, PROJECT, TASK AREA & WORK UNIT NUMBERS: Project No. 471, NR031-778
11. CONTROLLING OFFICE NAME AND ADDRESS: Office of Naval Research, 800 North Quincy Street, Arlington, Virginia 22217	12. REPORT DATE: (11) August 1979
	13. NUMBER OF PAGES: 101
14. MONITORING AGENCY NAME & ADDRESS (if different from Controlling Office): (12) 140p.	15. SECURITY CLASS. (of this report): UNCLASSIFIED
	15a. DECLASSIFICATION/DOWNGRADING SCHEDULE

16. DISTRIBUTION STATEMENT (of this Report)

Reproduction in whole or in part is permitted for any purpose of the United States Government.

17. DISTRIBUTION STATEMENT (of the abstract entered in Block 20, if different from Report)

18. SUPPLEMENTARY NOTES

19. KEY WORDS (Continue on reverse side if necessary and identify by block number)

Plasma arc welding, plasma diagnostics, atomic spectroscopy, least squares method, integral equations, statistical inference, titanium alloys.

20. ABSTRACT (Continue on reverse side if necessary and identify by block number)

A three-year study was made of physical phenomena underlying operation of the plasma-arc welding (PAW) process. Experimental methods were developed to measure plasma spectral intensities during welding, a mathematical method was perfected to compute plasma temperature distributions from the spectral data, and statistical methods were used to extract maximum information from the data and to infer improved values for four Ar_{II} transition probabilities. Welds in mild and stainless steels and in Ti-6Al-4V up to 12.7 mm thick were

DD FORM 1 JAN 73 1473 EDITION OF 1 NOV 65 IS OBSOLETE

UNCLASSIFIED

SECURITY CLASSIFICATION OF THIS PAGE (When Data Entered)

389 949

evaluated by metallography and/or by cyclic fatigue studies. At low stress concentration levels PAW was found to reduce cyclic crack growth rates in the weld metal compared to the parent metal. There appears to be evidence that plasma spectroscopy can aid in selection and control of welding parameters. The plasma temperature measurements clarify the mechanism whereby use of auxiliary ports in the PAW torch orifice cup reduces the width of a weld nugget. Simple plasmadynamic models were used to relate orifice geometry to plasma temperature and electrical resistance, and to weld quality, thus accounting for the observation that a convergent orifice enhances weld penetration, reduces weld width, and improves weld nugget geometry without causing double-arcing, while a divergent orifice (which simulates an eroded orifice cup) has the opposite, deleterious, effects. Nine documents are cited in which these results were reported and complete preprints of four journal articles not yet published are included as appendices.

CONTENTS

INTRODUCTION

The purpose of this research was to investigate the basic physical phenomena underlying operation of the plasma-arc welding (PAW) process, to identify parameters whose optimization achieves desired weld quality, and in particular to measure plasma temperature distributions in the standoff region and show the relationship of the temperature distribution to weld penetration and quality in the welding of 12.7 mm (half inch) thick Ti-6Al-4V. Progress towards this goal has been reported in the following documents:

1. C.B. Shaw, Jr., "Fundamentals of Plasma Arc Welding," renewal proposal, Contract N00014-75-C-0789, Project 471, Rockwell International Science Center document SC2709T, 25 February 1976.
2. C.B. Shaw, Jr., B.I. Davis and D.W. Trover, "Fundamentals of Plasma Arc Welding," annual report on Contract N00014-75-C-0789, Project 471, Rockwell International Science Center document SC5031.7AR, October, 1976.
3. C.B. Shaw, Jr., "Fundamentals of Plasma Arc Welding," renewal proposal, Contract N00014-75-C-0789, Project 471, Rockwell International Science Center document SC2832T, 11 March 1977.
4. C.B. Shaw, Jr., "Temperature Measurement in Welding Plasmas," poster session contributed paper, annual meeting, Plasma Physics Division, American Physical Society, 30 October – 3 November 1978, Colorado Springs, Colorado.
5. C.B. Shaw, Jr., "Statistical Inference of Four Ar_{II} Transition Probabilities," submitted for publication as a Note in J. Quant. Spectrosc. Radiat. Transfer, Rockwell International Science Center document SC-PP-79-72, August, 1979.

6. C.B. Shaw, Jr., "Effect of Orifice Geometry in Plasma-Arc Welding of Ti-6Al-4V," submitted for publication in Met. Trans. B, Rockwell International Science Center document SC-PP-79-73, August, 1979.

7. C.B. Shaw, Jr., "Determination of Temperature Distributions in Welding Plasmas," submitted for publication in IEEE Transactions on Plasma Science, Rockwell International Science Center document SC-PP-79-74, August, 1979.

8. C.B. Shaw, Jr., "Reconstruction of Certain Distributions from Very Limited Projection Data," submitted for publication in SIAM J. Num. Anal., Rockwell International Science Center document SC-PP-79-75, August, 1979.

9. C.B. Shaw, Jr., "Recent and Projected Research on Plasma Arc Welding of Thick Section Ti-6Al-4V," to be presented at the Naval Sea Systems Command's Workshop on Welding Technology of Thick Section Titanium Alloys, Annapolis, 18-19 September 1979.

The specific accomplishments reported in the above documents are summarized very briefly in the following section. Since the four preprints have not yet been published in their respective journals, they are included in their entirety as Appendices A-D. This work has led to a contract to study weld monitoring and control, which will be funded by DARPA and monitored by the Navy Sea Systems Command.

ACCOMPLISHMENTS

The following are the key results obtained in this study:

1. Numerous experimental obstacles to spectroscopic measurement of plasma temperature during welding were identified and means to circumvent them were found.
2. The mathematical technique for determination of plasma temperature from spectroscopic data was perfected.
3. The auxiliary ports sometimes used on either side of the main orifice in the PAW orifice cup were shown to narrow the weld by enhanced cooling of the base metal alongside the weld, not by cooling the plasma column nor making it more narrow as the manufacturer conjectures.
4. The feasibility of selecting the proper current for full-penetration welding at any selected travel speed and standoff distance by spectroscopic means was strongly suggested.
5. Argon ion spectral lines, seen clearly in the plasma near the torch, fade away near the workpiece; there the electron charge density is neutralized not only by argon ions but by more easily ionized metal vapor ions volatilized from the workpiece.
6. Cyclic fatigue studies indicate that the combinations of welding parameters selected as above are equally effective at producing refined welds of enhanced fracture toughness relative to the base metal.
7. Metallographic examination shows that use of a convergent orifice "focused" at the center of the workpiece gives enhanced penetration and improved nugget geometry.

8. Metallography shows that a divergent orifice, which simulates erosion due to prolonged use of the usual cylindrical orifice, causes loss of penetration and excessive top-bead width.

9. Plasma temperature measurements permit qualitative explanation of the preceding two results on the basis of "pneumatic constriction" of the plasma flow.

10. Statistical analysis of plasma diagnostic data yielded improved values for certain transition probabilities for four lines in the spectrum of ionized argon.

Ideally, a welding device would heat the base metal and any filler material to the liquidus, uniformly along the surfaces to be joined, without heating any metal but that melted. This would eliminate distortion, residual stresses, and degradation of the heat affected zone (HAZ), but requires a line-source of heat moving at infinite travel speed. In reality, imperfect joint preparation and fitup, and the need to control puddle circulation, mean that the highest available power density and travel speed may not give the best results. Even so, the controlled high power density achieved by the PAW torch is believed to be one of its principal virtues, which led to the decision to focus this research on measurement of plasma temperature during welding, and the correlation of temperature distributions with properties of the weldment. Photography of the plasma through narrow band thin film interference filters matched to specific spectral lines was expected to record at snapshot speed all data necessary for determination of a temperature distribution.[1,2] Earlier workers needed day-long observation of an artificially stabilized plasma to record comparable data.[3] Also, it had been observed mathematically that considerable asymmetry in the plasma could be resolved by observing it from only two view directions[4] rather than 37 directions or more.[5,6]

The apparatus described in Appendix C was therefore set up to photograph the plasma from two directions by the radiation from two spectral lines, in order to measure plasma temperature by the two-line method.[7] An iterative procedure (*cf.* Appendix D) was developed to determine the scale factor needed for analysis of the data,[4-6] and, with meticulous alignment of all optical elements, it was possible to perform the desired temperature measurements (Appendix C). These showed that the auxiliary ports (through which neutral gas flows on either side of the main orifice from which plasma flows) do not chill the plasma column and make it narrower, transverse to the line of welding, than it is long, along the line of welding, as the torch manufacturer states. Instead, the auxiliary ports make the weld narrower by aiding the cooling of the workpiece on either side of the fusion zone and HAZ. This is in accord with the previous demonstration, by means of holographic interferometry, that heat flows into the workpiece from the plasma, but then through the workpiece and back into neutral gas immediately surrounding the ionized region.[8] In the plasma itself, the major departure from axial symmetry is an increase in temperature gradient in front, where cold metal is moving under the torch, and a decrease in gradient behind, where hot metal moves away from the torch, the difference in temperature of the metal boundary being reflected in the temperature distribution of the plasma. This confirms our belief that the behavior of the weld metal directly influences the plasma temperature distribution, and can be monitored by observation of the plasma spectrum.

The apparatus described in Appendix C used mirrors to fold the optical paths so that the two view directions appeared to be separated by only 3° instead of the actual 87°. This still avoided overlapping of the pairs of arc images, as seen from the two directions, but permitted use of a single two-wavelength camera in which the apparent source

directions were 1.5° on either side of the camera's optical axis. This use of a single camera system proved to be grossly false economy. It is true that at about 1.5° off normal incidence (for the bandwidth, effective index of refraction, and number of interferometer cavities in our filters) transmission is greater than 90% of the peak value for normal incidence,[9] but our measurements showed that the transmittance became a rapidly-varying function of angle just beyond that value. This meant that satisfactory alignment of the system was quite difficult and that minor drift in the alignment (due to elastic relaxation of mounts, differential thermal expansion, or vibration) put one path or the other of the system into the self-vignetting regime, where the percentage of transmission for light from one part of the source is not the same as for another part of the source. Another false economy was use of only two spectral lines instead of several lines[7] for temperature determination. This meant that only one beam splitter and two narrow band filters and camera bodies were required instead of, say, three beam splitters and four filters and camera bodies, but the simplification left our data precariously poised on the brink of nonsense. It had been realized that the transition probabilities, needed to compute temperature by comparison of local emission coefficients for the different spectral lines, were known only to within 10% at best. However, it was felt this would permit useful determination of relative temperatures, as influenced by changes in welding parameters, which could be correlated with properties of the weldment, even if the absolute values of the temperatures were in error. All too often, however, such comparisons and correlations were frustrated when a key set of data proved, after reduction and analysis, to indicate that the temperature went to infinity with increasing radius along some azimuth, or was negative. Realignment and recalibration were then necessary.

The first renewal proposal[10] and first annual report[11] describe the methods developed to align the system and to determine magnification, view angle, position in a fixed coordinate system, and overall transmission for each image, to calibrate the scanning microdensitometer used to measure the processed film, and determine the actual film calibration curve (log exposure versus density).

As reported in the second continuation proposal,[12] the identification of a common coordinate system for sets of images was further refined the second year, to avoid problems of image mis-registration which accounted for some of the un-physical temperature measurement results. An even more important change was use of filters to select lines in the near infrared spectrum of neutral argon (Ar_I) instead of visible lines of ionized argon (Ar_{II}). The latter lines have superimposed on them continuum radiation whose contribution to film density must be corrected for in order to compute the plasma temperature. The Ar_I lines are free of continuum. This is particularly important when temperature is to be measured throughout the plasma. Correction for the continuum had depended on spectrographic measurement of intensity as a function of wavelength and of position in a single horizontal slice through the plasma, the spectrograph and set of images being recorded simultaneously. A technique was developed which made it possible to change quickly and accurately the vertical position of the slice sampled by the spectrograph, and several exposures could be made during a single welding run. Near the torch, the spectrograms showed that the continuum was weak compared to Ar_{II} line intensities. It was felt therefore that inability to resolve asymmetry from a single spectrographic view of the plasma did not seriously impair the accuracy of the small correction. Halfway down the plasma, however, the Ar_{II} lines weakened to the point where continuum radiation, integrated across the passband of the narrow band filter, was as strong as the line intensity. This is indirect evidence of the significant presence of

ionized metal vapor in the lower portion of the plasma. (The Saha equation, from which one computes the degree of ionization, is simply the chemical mass-action law applied to the "chemical" equilibrium of neutral atom versus ion plus electron.[7] It follows that the density of metal ions will be greater than the density of argon ions whenever the ratio of neutral metal density to neutral argon density is greater than the ratio of the mass-action constant for ionization of argon to the constant for ionization of metal vapor. This last ratio is very small, being proportional to the exponential of the difference in ionization potentials in units of kT.) Use of the Ar_I lines obviated this entire problem. Furthermore, it eliminated a weak link in film and transmittance calibrations. Standard light sources available for these calibrations were not bright enough at the Ar_{II} wavelengths to permit calibration exposure times to be as short as plasma exposure times. This required adjustment of the film calibration curve for reciprocity failure. (Reciprocity is the approximation that final film density depends only on the product of intensity and exposure time, not on these two variables independently.) The Ar_I wavelengths are so much closer to the peak spectral radiance of the incandescent standard sources and the Ar_I line intensities are sufficiently weaker than Ar_{II} intensities, that the same exposure times could be used for calibration exposures and plasma exposures. This eliminated reciprocity problems.

While awaiting delivery of sheets of Ti-6Aℓ-4V of proper thicknesses and their fabrication into weld specimens, welds were made in AISI 1018 mild steel and AISI 304 stainless steel to pursue correlation of key features of plasma temperature distributions with weldment properties. Unfortunately, now physically unrealistic calculated temperatures became even more frequent. This was due to the extreme difficulty of maintaining the critical 1.5° angle between optical axis and view direction, as previously discussed, for wavelengths to which the human eye does not respond. An attempt was made to use a silicon vidicon camera, sensitive

out to 1.1 μm, to aid in the alignment, but to no avail. Successful alignment, and therefore temperature measurement, was possible but not reliably so, and failure could not be detected until long after the experiments had been completed. Systematic exploration of the desired correlations between temperature and weldment characteristics were thus frustrated. Many boxes in the test plan matrix could not be filled, and the error bars on those measurements whose results seem reasonable are uncomfortably large. Therefore, the following remains a conjecture rather than a proven fact. It seems to be that the plasma temperature near the torch orifice is minimized by choosing a value for one welding parameter (e.g., current) which barely achieves full penetration with other parameters (e.g., travel speed, standoff distance, gas flow rates) held constant. Moreover, each combination of parameters which produces such a minimum gives equally satisfactory welds. If variation of the one welding parameter has a strong effect on plasma temperature, it also has a strong effect on the weld. This pairing of strong effects was seen, for example, when current was varied in order to achieve full penetration at the highest travel speed used. The current had to be controlled to within 1 or 2 amperes to maintain full penetration without excessive drop through; at lower travel speeds, the tolerance was 5 amperes.

In addition to the usual transverse sectioning, polishing, and etching to verify penetration and depth-to-width ratio of the weldment, some welds were sectioned longitudinally along the center line of welding to check variability of penetration. Variability of penetration also seemed to be associated with variability in the measured plasma temperature, for welding parameters which nominally were being held constant.

As in a parallel program which studied PAW of Inconel 718,[13] specimens of AISI 304 stainless steel on which full penetration welds had been

made, using various combinations of travel speed and current, were fabricated into compact tension specimens. The specimens were precracked to form a sharp notch and the cracks were propagated under controlled 10 Hz cyclic loading, the ratio of minimum to maximum load being 0.1. Cracks were propagated both in the weld metal and in the parent metal. The HAZ was not large enough nor uniform enough to be tested. Log-log plots of the crack propagation rate da/dN versus change in stress intensity ΔK showed no significant variation from one set of welding parameters to another. For low values of ΔK, however, the cracking rate was higher in the parent metal than in the weld metal. This indicates that PAW is a refining process which toughens the metal against cyclic cracking. These results will not be published because the Inconel 718 data is more convincing, showing as it does that the HAZ has a crack rate intermediate between that of the welded and parent materials.

As is detailed in Appendix B, the third year's study of the effects of orifice geometry on PAW of half-inch Ti-6Al-4V showed conclusively the advantage of using a conically convergent orifice rather than the usual cylindrical orifice, and the complementary disadvantage of using a divergent orifice — which simulates erosion of a normal orifice operated too long or at too high a current level. The simple precaution of abrasively polishing the exit port smooth avoided deleterious double-arcing when the convergent orifice was used. A set of simple mathematical models of the plasmadynamic effects of the alternative orifice designs showed that the concept of pneumatic constriction tied together all the observed effects of orifice geometry on plasma temperature and electrical resistance, and on weld penetration, width, and shape.

Statistical methods were used extensively in this study to seek out systematic error sources. Regression analysis of the residual differences between observed and theoretically fitted values of spectral line intensities

permitted improvement in the accuracy of film calibration curves (Appendix C). As an unexpected benefit of this research, significantly improved values for the transition probabilities of four Ar_{II} spectral lines were inferred statistically from the plasma temperature measurement data (Appendix A). For this final effort, temperature measurements were restricted to welding parameters for which the plasma could be approximated as being cylindrically symmetric, so that only a single view direction was required. The spectrographic method, rather than photography through thin film filters, was used to record data for one horizontal slice at a time. This avoided both the difficulty in aligning the system for infrared Ar_I lines, and the difficulty in making the continuum correction for visible Ar_{II} lines. Moreover, the line and continuum intensities for four, rather than two, Ar_{II} spectral wavelengths were used systematically, which significantly improved the accuracy of the plasma temperature measurements.[7]

REFERENCES

1. C.B. Shaw, Jr. and B.I. Davis, "Time-Resolved Temperature and Density Distribution in a Welding Arc," Conference Record, First International Conference on Plasma Science, IEEE Publication 74CH0922-5-NPS, 15-17 May 1974, p. 13.

2. C.B. Shaw, Jr., "Diagnostic Studies of the GTAW Arc," Welding J. *54* (2) 33s-44s, *54* (3) 81s-86s (1975).

3. H.N. Olsen, "Thermal and Electrical Properties of an Argon Plasma," Phys. Fluids *2* 614-623 (1959).

4. C.B. Shaw, Jr., "Reconstruction from a Few Imperfect Projections," in R.B. Marr, ed., *Techniques of Three-Dimensional Reconstruction*, Proc. Int'l. Workshop 16-19 July 1974, Brookhaven National Laboratory Report BNL 20425 (1974).

5. C.D. Maldonado and H.N. Olsen, "New Method for Obtaining Emission Coefficients from Emitted Spectral Intensities. Part II — Asymmetrical Sources," J. Opt. Soc. Am. *56* 1305-1313 (1966).

6. H.N. Olsen, C.D. Maldonado, and G.D. Duckworth, "A Numerical Method for Obtaining Internal Emission Coefficients from Externally Measured Spectral Intensities of Asymmetrical Plasmas," J. Quant. Spectrosc. Radiat. Transfer *8* 1419-1430 (1968).

7. W. Lochte-Holtgreven, "Evaluation of Plasma Parameters," in W. Lochte-Holtgreven, ed., *Plasma Diagnostics*, Ch. 3, John Wiley and Sons, New York (1968).

8. C.B. Shaw, Jr. and B.I. Davis, "Diagnostic Arc Studies with Ruby Laser," Proc. Soc. Photo-Opt. Inst. Eng. *41* 89-99 (1973).

9. Albert A. Kusch, "Matching Interference Filters to Avoid Vignetting," Laser Focus *12* (1) 62-66 (1976).

10. C.B. Shaw, Jr., B.I. Davis, and D.W. Trover, Rockwell International Science Center document SC2533T (1975).

11. C.B. Shaw, Jr., B.I. Davis, and D.W. Trover, Rockwell International Science Center document SC5031.7AR (1975).

12. C.B. Shaw, Jr., B.I. Davis, and D.W. Trover, Rockwell International Science Center document SC2832T (1977).

13. C.B. Shaw, Jr. and Wayne Robertson, Rockwell International Science Center IR&D Technical Plan, Project 815, pp. 2-131 to 2-161 (1977).

APPENDIX A

STATISTICAL INFERENCE OF FOUR AR_{II} TRANSITION PROBABILITIES

Rockwell International Science Center document SC-PP-79-72, submitted for publication as a Note in J. Quant. Spectrosc. Radiat. Transfer

NOTE

STATISTICAL INFERENCE OF FOUR Ar_{II} TRANSITION PROBABILITIES

C.B. SHAW, JR.

Rockwell International Science Center
P.O. Box 1085
Thousand Oaks, California 91360

Abstract — Using the multi-line method, several hundred temperature measurements were made in a partially stabilized high pressure argon arc. Statistically significant evidence requires revision of transition probabilities for the Ar_{II} lines at 476.489, 480.607, 484.790, and 487.990 nm.

Spectroscopic measurement of temperature distributions in a high-pressure flow-stabilized argon arc was undertaken for diagnostic purposes, as part of an investigation into the physical foundations

of the plasma-arc welding process.[1-3] To idealize somewhat, the discharge is between a cylindrical tungsten cathode with conical tip, and a ring anode. The cathode is surrounded by a copper cup, which contains an orifice that is coaxial with the cup, with both electrodes, and with the axis of symmetry of argon streamlines. A low-subsonic flow of argon passes inside the cup, along the cathode, through the orifice, toward and finally through the ring anode. A ballast resistor between cup and anode completes the circuit for passage of a small "pilot arc" current from cathode to cup, to pre-ionize gas flowing to the orifice, but the primary current path from cathode to anode is through the flowing plasma.

Deviations from the simple axisymmetric case described above are of technological significance.[1] A spectroscopic measurement method was therefore devised to cope with quite asymmetric plasmas by means of special experimental[2] and analytical[3] techniques. However, a substantial body of data has been recorded for which the emitted radiation is indeed axially symmetric. Conventional Abel inversion rather than its generalization[3] can therefore be used to recover local emission coefficients from total projected intensities. Consider a Cartesian coordinate system in which the vertical axis of symmetry of the arc is the z-axis. The observation direction is the y-axis, so that the observed intensity

$g(x,z)$ is related to the local emission coefficient $f(r,z)$, independent of θ, by

$$g(x,z) = \int_{-\infty}^{\infty} f(r,z)dz \qquad (1)$$

with $r^2 = x^2 + z^2$. The arc was imaged, with magnification 1.5 times, onto the entrance slit of a 0.3 m Czerny-Turner monochromator (modified for use as a spectrograph). A Dove prism was used to rotate the image 90° about the y-axis so that the entrance slit defined a small range Δz at z, with x now designating vertical position on the entrance slit, and on the film, normal to the dispersion direction. A micrometer drive moved the monochromator horizontally between exposures to vary z. After processing, the film was scanned by a microdensitometer with rectangular aperture, adjusted to give good resolution in x while integrating over the full width of each spectral line. The nominal film calibration curves used to relate density to log(exposure) could be refined from frame to frame by statistical means.[2] Each value for the intensity of a spectral line was corrected by subtraction of the average continuum intensity, as measured on either side of the line. For a certain range of operating parameters, the data were observed to be well described by

$$g(x,z) = g_0(z) \exp\left[-\alpha^2(z)x^2\right] . \qquad (2)$$

It follows from Eq. (1) that, in these cases, the local emission coefficient for the i^{th} spectral line depended on position as

$$f_i(r,z) = \pi^{-\frac{1}{2}}\alpha_i(z)g_{0_i}(z)\ \exp\ [-\alpha_i^2(z)r^2] \tag{3}$$

with α_i and g_{0_i} the values fitted to data for line i as in Eq. (2).

The temperature T(r,z) could now be found by the multi-line method.[4] Suppressing the (r,z) notation on f_i and T, one has[4]

$$f_i = \frac{bA_ig_in(T)}{u(T)\lambda_i}\ \exp\ (-E_i/kT) \tag{4}$$

where n(T) and u(T) are the total particle density and partition function of the plasma, b and the Boltzmann constant k are universal constants and, for each line, A_i is the Einstein spontaneous emission coefficient for the atomic transition producing wavelength λ_i, and g_i and E_i are the degeneracy and energy of the upper state from which the transition takes place. It follows that if the logarithm of the weighted emission ϕ_i, defined by

$$\phi_i \equiv f_i\lambda_i/g_iA_i \tag{5}$$

is plotted against E_i, then the slope m of a straight-line fit to the data:

$$\log \phi_i \sim a + mE_i \tag{6}$$

for i = 1,2,···,N gives the temperature as:

$$T = -1/km \ . \tag{7}$$

Figure 1 shows a typical example of our log ϕ_i versus E_i data. The observed values are marked by crosses, the fitted values by the solid line. The pattern of residuals, r_i, defined by:

$$r_i = \log(\phi_i) - (a + mE_i) \tag{8}$$

was observed to repeat with striking regularity for each line λ_i, regardless of position or values of arc operating parameters. Using all available data suitably described by Eq. (2), a test[5] based on Student's t strongly rejects the null hypothesis that the observed residuals for each line are samples from a population of zero mean — no correction needed for the given line. Our data therefore indicate errors in the published values[6] of the transition probabilities which were used in Eq. (5), if one

assumes λ_i and g_i to be correct. The corrections are indicated in Table I, together with the confidence level[7] at which the null hypothesis was rejected. These results are based on seventeen independent experiments in which the intensities of Ar_{II} lines, after correction for film calibration errors, were used to find the temperature at a total of 454 points. In Figure 1, the circles show log ϕ_i versus E_i when each A_i is adjusted, as indicated by the mean value of r_i, to the values shown in Table I.

Acknowledgement — This work was supported in part by Rockwell International under its Independent Research and Development Program, and in part by the U.S. Navy, Office of Naval Research, Project 471, under contract N00014-75-C-0789. The author is deeply grateful to B.I. Davis for invaluable assistance.

REFERENCES

1. C.B. Shaw, Jr., Effect of Orifice Geometry in Plasma-Arc Welding of Ti-6Aℓ-4V, Rockwell International Science Center preprint SC-PP-79-73, submitted for publication in Met. Trans. (1979).
2. C.B. Shaw, Jr., Determination of Temperature Distributions in Welding Plasmas, Rockwell International Science Center preprint SC-PP-79-74, submitted for publication in IEEE Transactions on Plasma Science (1979).
3. C.B. Shaw, Jr., Reconstruction of Certain Distributions from Very Limited Projection Data, Rockwell International Science Center preprint SC-PP-79-75, submitted for publication in SIAM J. Num. Anal. (1979).
4. W. Lochte-Holtgreven, "Evaluation of Plasma Parameters," in W. Lochte-Holtgreven, ed., Plasma Diagnostics, Chapter 3, p. 181, John Wiley and Sons, New York (1968).
5. John F. Kenney, Mathematics of Statistics, Part Two, Chapter VII, D. Van Nostrand Company, New York (1941).
6. Rudolf Schnapauff, Über Messungen von A II Übergangswahrscheinlichkeiten und die Kontinua von A und Ne, Z. Astrophys. 68, 431-444 (1968).
7. M. Abramowitz and I.A. Stegun, eds., Handbook of Mathematical Functions, Chapter 26, National Bureau of Standards, Washington, D.C. (1964).

Fig. 1. Typical log (weighted intensity) with (0) and without (X) correction of A_i by average residual for all measurements of line i.

Table I. Transition Probabilities A_i for Ar_{II} Lines Corrected by Regression Analysis

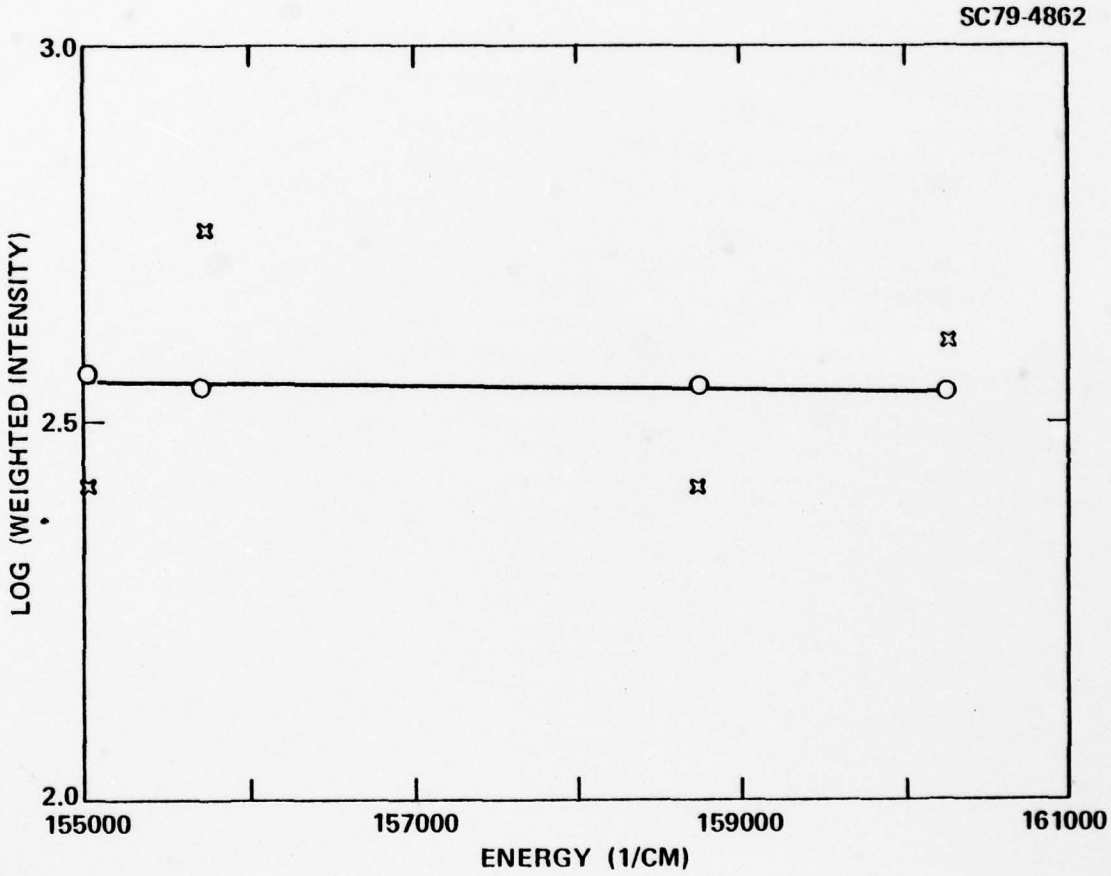
SC79-4862
3.0
2.5
2.0
LOG (WEIGHTED INTENSITY)
155000
157000
159000
161000
ENERGY (1/CM)

Line	Wavelength (nm)	A_I (10^7/sec)		Published Error Limit	Correction	Student t	Confidence
		Published	Corrected				
1	476.489	4.37	4.82	25%	+10.2%	55.77	> 99.99999%
2	480.607	5.70	5.62	10%	-1.5%	-4.04	99.99986%
3	484.790	6.44	6.88	25%	+6.8%	13.58	> 99.99999%
4	487.990	5.52	4.75	25%	-13.9%	-54.05	> 99.99999%

APPENDIX B

EFFECT OF ORIFICE GEOMETRY IN PLASMA-ARC WELDING OF Ti-6Aℓ-4V

Rockwell International Science Center document SC-PP-79-73, submitted for publication in Met. Trans. B

EFFECT OF ORIFICE GEOMETRY IN PLASMA-ARC WELDING OF Ti-6Aℓ-4V

C.B. Shaw, Jr.

Rockwell International Science Center

Thousand Oaks, California 91360

Abstract — Comparisons have been made among the performances of three plasma-arc welding torch orifice geometries: conically convergent, conventional cylindrical, and conically divergent. The minimum orifice diameter and all welding parameters (including constant torch-to-workpiece distance rather than constant voltage) were identical for the three designs when test butt welds were made in Ti-6Aℓ-4V up to 12.7 mm (0.5 in.) thick. Measurements were made during welding of the plasma voltage drop and plasma temperature distribution. The resultant weldments were cross-sectioned and examined. Compared to the standard orifice, the convergent design produces a greater voltage drop, higher plasma temperature, deeper weld penetration, and smaller nugget width-to-depth ratio. The divergent design has the opposite effect on all these points. A complete plasmadynamic analysis has not been made, but analysis of simple models relates all these phenomena to "pneumatic constriction" produced by flow through the convergent orifice.

INTRODUCTION

The plasma-arc welding (PAW) process is distinguished from the gas tungsten-arc welding (GTAW) process by the presence of an orifice cup which surrounds the tungsten electrode, normally the cathode, common to both processes. The melting workpiece normally serves as anode in the arc discharge through flowing inert gas, e.g., argon. A small pilot-arc current, limited by the series resistor which connects the orifice cup to the workpiece, flows between electrode and orifice cup to pre-ionize

the gas flowing out through the orifice, but the major current flow between electrode and workpiece is constrained to pass through the plasma which streams through the orifice toward the workpiece. The tungsten electrode, a cylinder with a broad conical tip, the orifice and the axis of symmetry of gas and current flow, are all coaxial.

The welding performance of a PAW torch is well known on empirical grounds to be superior in several ways to that of a GTAW torch,[1] a superiority which is popularly attributed to "constriction" of the arc discharge by causing the plasma to flow through the orifice. In view of this central importance of the orifice to PAW performance, published research on the effects of orifice geometry and its optimization seem surprisingly scant. Demyantsevich and Sosnin[2] included orifice geometry among the variables they explored in a search for a more "efficient" plasma torch, using concentration of heat flux and current flow to measure efficiency. They studied both convergent and divergent orifices, the latter including a paraboloid of revolution chosen to simulate erosion of the orifice cup through prolonged use. No evaluation of actual welds was presented, but by their measure of efficiency the performance of a divergent orifice is inferior, that of a convergent orifice superior to that of a cylindrical orifice, and the use of tangential gas feed and an annular electrode is better yet.

Schultz's group[3] reported an extensive metallographic evaluation of the effects of orifice geometry on weld nugget morphology and explored the range of welding parameters over which each design permitted satisfactory welding performance. Clear superiority was shown for a design based on

the concept of "striction pneumatique" (pneumatic constriction) which used a conically convergent orifice section. However, to avoid the problem of double arcing — in which the main current flow goes from the electrode to a spot on the orifice cup and from there to the workpiece — which causes erratic welding and rapid orifice-cup deterioration, they followed the convergent orifice with a conically divergent section at the outlet. A similar design concept was used to achieve the greatest single-pass penetration depths yet attained by the PAW process in the welding of titanium and steel alloys.[4]

Schultz discussed qualitatively the effects of orifice geometry on gas flow, but neither measured nor analyzed the flow.[3] The present work was therefore undertaken to supplement metallographic observation of the effects of orifice geometry on welds in Ti-6Al-4V by measurement of plasma temperature distributions produced by the various orifice shapes and by gasdynamic modelling of the flows. The objective was to explore the physical mechanisms whereby a convergent orifice produces welds which are superior to those made by a cylindrical orifice using the same welding parameters, while a divergent orifice (e.g., one eroded by prolonged use) yields inferior results. The modelling has not been as successful as hoped, but the reasons for this and the limited results obtained are discussed below along with the experimental data.

EXPERIMENTS

Blank orifice cups were obtained from the torch manufacturer, and three types of orifices were machined in them: 1. A right circular conically convergent orifice, the cone having 15° included angle.

2. A straight right circular cylindrical orifice. 3. A right circular conically divergent orifice, the cone again having 15° included angle. These will be referred to as -15°, 0°, and +15° tapers, respectively. (Additional orifices with +30° and +45° tapers were also produced but quickly dropped from the test program; they produce welds so broad that excessive sag and even cutting result before full penetration welds can be obtained.) The minimum diameter of each orifice was 3.45 mm (0.136 in.), the diameter recommended by the manufacturer for the intended current range. The edges at the entrance and exit of each orifice were polished smooth with abrasives. This was done on the assumption that double arcing is engendered by electric field concentration, which is known to be significant at a sharp edge or the point of a burr on a conductor.[5] No double arcing was encountered, even with the -15° taper.

Single-pass butt welds were made on Ti-6Al-4V bar stock, each strip being 38.1 by 305 mm (1.5 in. by 12 in.), with thicknesses from 3.2 to 12.7 mm (0.125 to 0.5 in.). The edges to be joined were filed clean and smooth immediately before clamping the specimens to the water-cooled grooved copper back-up bar. The bars were tack-welded together with a gap of 0.36 mm (0.014 in.). All welds were made in an inert-atmosphere chamber filled with argon to prevent oxidation and nitridation of the hot titanium. No shield-gas flow was therefore necessary, but the orifice flow rate was the normal value for full penetration welding in the keyhold mode.[1] Travel speed was selected in the range 50 to 400 mm/minute according to specimen thickness in order to keep the current in the range 40 to 120 amperes. Constant stand-off distance (from orifice to workpiece)

was used rather than automatic voltage control, the distance being 3.2 mm (0.125 in.) at low current and 6.3 mm (0.25 in.) for currents of 80 amperes and above.

For every combination of workpiece thickness, travel speed, and current employed, the following results were uniformly obtained. Relative to the 0° taper orifice, the -15° taper (convergent orifice) produced a plasma such that the potential difference between workpiece and electrode was 3 to 6% (1 to 2 volts) greater. That is, the plasma column had 3 to 6% higher overall electrical resistance and the electrical energy delivered per unit length of weld was correspondingly greater. The +15° taper (divergent orifice) produced a plasma for which the potential difference was reduced 6 to 10% (2 to 3 volts), indicative of correspondingly reduced overall electrical resistance and reduced electrical energy delivered per unit length of weld.

Measurement of the plasma temperature distributions[6] showed that the plasma produced by the -15° orifice was 8 to 12% (2.5 to 3.8 $\times 10^3$ K) hotter than that from the 0° orifice, while the plasma from the +15° orifice was 20 to 30% (6.3 to 9.5 $\times 10^3$ K) cooler than the reference. The full width at half maximum of the temperature distributions did not depend significantly on taper, but the radius at which the intensity of the measured spectral lines dropped to the smallest useful value was less for the -15° taper and greater for the +15° taper than for 0°. Typical results are shown in Figure 1. The temperature in thousands of degrees Kelvin is plotted against distance in millimeters from the torch axis of symmetry, as measured 0.97 mm below the torch orifice while welding 5.3 mm (0.21 in.) thick Ti-6Al-4V at 70 amperes and 8 in. per minute. The standoff distance

was 3.2 mm (0.125 in.). The measured voltages were 34, 32 and 28 volts for the -15°, 0°, and +15° orifice tapers, respectively.

For every set of welding conditions the -15° taper gave deeper penetration and a smaller average ratio of width to depth than the 0° taper. The +15° taper gave shallower penetration and a much greater ratio of width to depth. Quantitative comparison is limited by the frequent production of pipe defects in the welds. In order to make the most direct comparison of the effects of orifice geometry, it was decided to accept defects as they came, rather than to adjust orifice gas flow rate according to the weld penetration achieved by each orifice design. The pipes, which are continuous voids parallel to the line of welding and extend for many millimeters, are not infrequently produced in PAW when the orifice gas flow rate is adjusted for full penetration keyhole-mode welding but the current is insufficient to achieve full penetration. Their presence cannot be detected until the weld is radiographed or sectioned. Once thermal expansion closes the initial gap between plates the vigorous flow of argon into the weld pool can produce a bubble of appreciable size within the circulating weld metal, which flows above the gas to a cooler region where it solidifies. The pipe marks the location in which argon (together with surface tension and inertia) was supporting the molten metal. Figures 2-4 show polished and etched sections of welds made at 90 amperes and 2 in. per minute in 12.7 mm (0.5 in.) Ti-6Aℓ-4V, using the -15°, 0°, and +15° tapers, respectively. The standoff distance was 6.3 mm (0.25 in.). A pipe is clearly visible in the 0° specimen. The fusion zone is delimited by the boundary between large columnar solidification grains and the smaller

equi-axed grains of the inner heat affected zone, which underwent transition to the β phase. Figure 2 shows that the -15° taper achieved full penetration, producing a nugget 8.4 mm wide at the top (0.66 times penetration depth), and 2.9 mm at the bottom, for an average width of only 5.6 mm, which is 0.44 times the penetration depth of 12.7 mm. There is a slight drop-through of 0.2 mm, and undercutting to a depth of 0.4 mm along either edge of the weld. As shown in Figure 3, the 0° taper produced penetration to 11.4 mm, 10% less than full penetration. The nugget width at the top is 9.00 mm, or 0.79 times the penetration depth. There is no undercutting. The pipe is 2.1 mm wide and 1.4 mm high, with an area of approximately 2.3 mm^2; this accounts for approximately 1/3 of the cross-sectional area of the raised top-bead of 7.7 mm^2, the rest being attributable to shrinkage. Figure 4 shows that the +15° taper produced a weld nugget 13 mm wide at the top surface, 1.4 times the maximum penetration depth of only 9.5 mm. These last measurements are less precise than the preceding ones, since the wide flat top surface of the weld was roughly rippled, and a section taken elsewhere in the weld would show slightly different values for depth and width.

ANALYSIS

The plasmadynamic equations and boundary conditions governing flow in a channel with conductive walls, such as the PAW orifice, are well understood even when an interior boundary exists (such as the tungsten electrode if it protrudes into the orifice), and numerical methods for their solution have been thoroughly explored and critiqued.[7] The corresponding equations and boundary conditions for the standoff region (between torch and workpiece)

are more difficult to analyze because of the increased difficulty in determining the electric field and treating computationally a boundary condition at infinity, but they have also been mastered, at least in an approximation which neglects turbulence.[8] What cannot be treated correctly at the present time is the abrupt transition from channel flow to free flow which takes place at the outlet of the orifice. An attempt was made to match numerical solutions for flow in the two regions by only requiring that the total rates of transport of mass, charge, momentum, and energy by the two flow fields should match at the outlet, instead of requiring that they coincide point by point. The results obtained, however, were not physically significant; for example, the computed density field oscillated in such a way as to include negative values. It is believed that this failure stems from neglect of turbulence (which destroys axial symmetry of the flow) generated by the abrupt transition at the orifice. In reality, it is known experimentally that any atmospheric-pressure arc discharge which is not stabilized by presence of a wall or by some artifice is highly turbulent.[8] (Reference 8 refers to a "TIG* similar arc," rather than to a TIG arc, because an artifice was used to suppress turbulence.) Rather than attempt analysis of a three dimensional turbulent

*The American Welding Society recommends use of the term "GTAW" rather than the older term "TIG," which stands for tungsten inert gas, to denote the process.

plasmadynamic flow, it was decided to see what could be inferred about the effect of orifice geometry on PAW by modelling simpler flow problems.

Inspection of the plasmadynamic equations for channel flow[7] shows that the trends of variation in the flow velocity field u, pressure p, sound speed a, temperature T, and density ρ with changes in channel cross-sectional area A should be in the same direction as in the much simpler case of flow of an un-ionized gas. A lower bound on the effect of orifice geometry on the flow field was therefore found by neglecting ohmic heating, dissipative processes such as viscosity, heat conduction, ionization and electromagnetic forces, and calculating just the effect of the three orifices on adiabatic and isentropic flow of a perfect gas. Conservation of mass means that the mass m' of gas flowing through any cross section A per unit time is independent of axial position in the orifice. In particular,

$$m' = \rho A u = \frac{pAu}{RT} \tag{1}$$

at the exit of the 0° taper orifice, the right-hand expression following from the perfect gas law. (Note that R here is not the gas constant but that quantity divided by the molecular weight of argon.) Equation (1) permitted u to be calculated from known quantities since m' can be found from the measured orifice gas flow rate in cfh or cubic meters per second, the static pressure p can be taken as approximately one atmosphere, and T was measured. The remaining one-dimensional gasdynamic equations[9] (which ignore any variation in flow variables transverse to the axis of the

orifice) as applied to flow through a channel of variable area[10] then permitted calculation of the reservoir or stagnation temperature and all flow variables at the entrance to the 0° orifice. It was verified that the flow was in the far subsonic region, u less than 0.01 a. Assuming that gas conditions were approximately the same at the entrance to all three orifices, it follows that the convergent orifice would cause the temperature to be higher at the orifice exit than would the straight orifice, whereas the divergent orifice would cause the exit temperature to be lower. This is in qualitative agreement with the experimental results. Given identical initial conditions, the convergent orifice would also produce higher dynamic pressure, $\frac{1}{2}\rho u^2$, at the outlet than the straight orifice while the divergent orifice would produce a lower dynamic pressure. This trend in dynamic pressure means that the stream from the convergent orifice would support a greater head of molten metal and thus enhance penetration, while the stream from the divergent orifice would support a lesser head, to the detriment of penetration. The empirical fact that the convergent orifice produced a plasma of higher resistance, higher voltage, and therefore higher energy per unit length of weld, while the divergent orifice had the opposite effect, also contributes to the observed effect on penetration — one cannot judge the relative importance of the two effects.

Although the above trends coincide qualitatively with the experimental results, they are at odds quantitatively. The temperature differences computed from the one dimensional gasdynamic equation for adiabatic isentropic flow of an ideal gas were less than one degree Kelvin instead of the thousands of degrees observed. Likewise, the computed dynamic

pressures for the -15°, 0°, and +15° orifices were 7, 5, and 2 Nm^{-2}, almost two orders of magnitude too small to account for the effect on penetration via hydrostatic support of molten metal. These quantitative discrepancies must be attributed to the gross oversimplification of neglecting ohmic heating and heat conduction.

It is somewhat surprising that the hotter plasma was found to have the higher overall resistance. If one had a uniform plasma of area A and length L, the overall resistance R would be

$$R = \eta L/A \tag{2}$$

where η is the electrical resistivity. For a fully ionized plasma, η is proportional to $T^{-3/2}$.[11] For a weakly ionized plasma the dependence is less simply expressed, but η decreases with increasing T.[12] (A plasma is "fully" ionized, i.e., dominated by Coulomb collisions rather than by collisions between charged and neutral particles, when the degree of ionization is more than about 1%.[13] For pure argon at one atmosphere pressure, this requires a temperature between ten and twenty thousand degrees Kelvin.) It must be, therefore, that the effective area of the plasma is changed more than the resistivity by use of the convergent or divergent orifices. This of course is in accord with the concept of pneumatic constriction.[3] Indeed, the breadth of the region emitting the ionized-argon spectral radiation used for temperature measurement[6] was roughly 10% less for the convergent orifice and 10% more for the divergent orifice than for the straight cylindrical orifice. These differences in diameter of the plasma

column imply a 20% change in area A. The plasma temperature differences were about 10%, which implies a 15% change in resistivity in the "fully" ionized region, so that according to Eq. (2) the resistance of the plasma produced by the convergent orifice should have been higher by some 5%, and that from the divergent orifice lower by some 5%, compared to the cylindrical orifice. This is consistent with the observed changes.

The reduction in area by pneumatic constriction also tends to account for the observed differences in plasma temperature, even though the minimum orifice cross section was the same for all three orifices. Neglecting conduction and compression or expansion, the rate of change of temperature T' for a unit mass of gas is

$$T' = \frac{q}{\rho c_p} = \frac{\eta j^2}{\rho c_p} = \frac{\eta I^2}{\rho c_p A^2} \tag{3}$$

where q is the rate of generation of thermal energy by ohmic heating, j is the current density and I the total current. But it has already been noted that

$$\eta = kT^{-3/2} \tag{4}$$

with k a constant, and if t is a characteristic time for heating the gas, roughly the same for all three orifices since the mass flow rate and minimum orifice area are the same, T' is related to the final temperature T by

$$T' = T/t \ . \tag{5}$$

Substitution of Eq. (4) and (5) into (3) gives

$$\frac{T}{t} = \frac{kT^{-3/2}I^2}{\rho c_p A^2} \tag{6}$$

or

$$T = \left(\frac{ktI^2}{\rho c_p}\right)^{2/5} A^{-4/5} \ . \tag{7}$$

The observed change of some 20% in A would then account for a change in the opposite direction of some 16% in T, certainly close enough to the observed results, considering the crudeness of this analysis.

Quantitative understanding of the effects of pneumatic constriction requires the plasmadynamic analysis of flow through and out of the orifice, including the effect of the abrupt transition from channel flow to free flow, which has not yet been accomplished. However, it can be noted in closing that if the flow were collisionless (which of course it is not) the velocity vectors of all particles emerging from the orifice would be confined to a cone whose axis is the torch axis of symmetry and whose outer limit is the extension of the conical surface of the orifice. For the 15° convergent orifice, the radius of this flow field would vanish at a distance z_0 from the torch, where

$$z_0 = 3.45 \text{ mm}/2 \tan 7.5° = 13.1 \text{ mm} \tag{8}$$

since the diameter of the orifice outlet is 3.45 mm and the included angle of the cone is 15°. (This happens to be very close to the center of the workpiece which is at 12.7 mm for the standoff distance of 6.3 mm (0.25 in.) and workpiece thickness of 12.7 mm (0.5 in.) used to produce the weld shown in Figure 2.) There would be a "line focus" of plasma from that point on along the axis, and — perhaps more realistically — the diameter of the plasma stream would already have been reduced 10% at a distance 1.31 mm from the torch.

CONCLUSIONS

The concept of pneumatic constriction qualitatively ties together several observed facts. A conically convergent PAW torch orifice produces a plasma which: (a) has reduced diameter and cross-sectional area, (b) has higher temperature in the standoff region, (c) has higher overall resistance and, for fixed standoff distance, (d) generates more energy per unit length of weld, (e) achieves greater penetration and (f) produces a desirably narrower weld with smaller ratio of the widths at top and bottom than a conventional straight cylindrical orifice. No trouble with double-arcing is observed if the orifice outlet is abrasively polished smooth and free of burrs; thus, it is not necessary to weaken the effect of the convergent orifice section by adding a final divergent section. The conically divergent orifice, which simulates the effect of orifice erosion, has the opposite, deleterious, effect in all details. A plasmadynamic analysis of flow through and out of the orifice is still needed for quantitative comparison with experimental measurements.

ACKNOWLEDGEMENTS

The author is deeply grateful to B.I. Davis for dedicated support and valuable original contributions to all aspects of the experimental work. D.W. Trover contributed both to laboratory work and to data reduction. W.E. Lawrence evaluated weld quality and offered valuable suggestions and encouragement. R.A. Spurling skillfully prepared metallographic specimens which J.C. Chesnutt carefully evaluated and interpreted. Useful discussions were held with S.S. Glickstein, T.W. Eagar, N.D. Malmuth, D.R. Brubaker and W.C. Perkins, and valuable suggestions as well as encouragement and support came from W.F. Hall, R.E. DeWames, B.A. MacDonald and J.C. Williams. This work was supported in part by Rockwell International under its Independent Research and Development Program, in part by the Air Force Materials Laboratory/LTM under Contract F33615-74-C-5036, and in part by the U.S. Navy Office of Naval Research, Project 471, under Contract N00014-75-C-0789.

REFERENCES

1. AWS Arc Welding and Arc Cutting Committee, *Recommended Practices for Plasma-Arc Welding,* publication AWS C5.1-73, American Welding Society, Miami, Florida, 1973.

2. V.P. Demyantsevich and N.A. Sosnin, "Some Ways of Increasing the Efficiency of the Plasma Arc," Welding Production *1974* (4) 26-29 (1974), Russian original Svar. Proiz. *1974* (4) 15-17 (1974).

3. P. Demars, J.-P. Schultz, and E. Cuny, "Les Nouvelles Possibilités du Procédé Plasma en Soudage," Soudages et Techniques Connexees *5/6* May-June, 211-230 (1973).

4. D.R. Brubaker, W. Padian, and P. Sidbeck, "Manufacturing Methods for Plasma Arc Welding," Final Report on Contract F33615-74-C-5036, Report AFML-TR-76-152, Air Force Materials Lab., September 1976 (AFML/LTM, Fred R. Miller, Program Manager, AF Materials Lab., Wright-Patterson AFB, Ohio 45433).

5. C.B. Shaw, Jr., "Diagnostic Studies of the GTAW Arc. Part 1 — Observational Studies," Welding J. *54* (2) 33s-44s; "Part 2 — Mathematical Model," Welding J. *54* (3) 81s-86s (1975).

6. C.B. Shaw, Jr., "Determination of Temperature Distributions in Welding Plasmas," submitted for publication in IEEE Trans. Plasma Sci. (Science Center Preprint SC-PP-79-74, C.B. Shaw, Jr., Rockwell International Science Center — A35, P.O. Box 1085, Thousand Oaks, California 91360) 1979.

7. K.V. Brushlinsky, "Numerical Simulation of Two-Dimensional Plasma Flow in Channels," Computer Meth. in Appl. Mech. and Eng. *6* 293-308 (1975).

8. K. Landes, G. Seeger, and W. Tiller, "Evaluation of Mass Flow Fields and Electric Current Density Fields in a Free Burning TIG Similar Arc," International Institute of Welding Document 212-462-79 (Prof. Dr.-Ing. Gerhard Seeger, Fachbereich Elektrotechnik, Hochschule der Bundeswehr Munchen, Werner-Heisenberg-Weg 39, 8014 Neufiberg, Federal Republic of Germany) 1979.

9. H.W. Liepmann and A. Roshko, *Elements of Gas Dynamics*, Wiley, New York, 1957, Ch. 2.

10. Liepmann and Roshko, *op. cit.* Ch. 5.

11. Lyman Spitzer, Jr., *Physics of Fully Ionized Gases*, Interscience, New York, 1956, Ch. 5.

12. H.W. Drawin, "Evaluation of Electrical Conductivity, Heat Conductivity and Viscosity of Plasmas," Ch. 15 of W. Lochte-Holtgreven, ed., *Plasma Diagnostics*, Wiley Interscience, New York, 1968.

13. Max F. Hoyarex, *Arc Physics*, Springer-Verlag, New York, 1968, Ch. 3.

FIGURES

1. Plasma Temperature versus Radius for Three Orifice Geometries, Temperature measured 0.97 mm Below Torch at 70 A, ○ = -15, □ = 0, Δ = +15 deg.
2. Weld Made in Ti-6Aℓ-4V 12.7 mm Thick with Convergent Orifice, Current 90 A, Travel Speed 0.85 mm/s, Standoff 6.3 mm.
3. Weld Made with Straight Orifice, Same Parameters as Figure 2.
4. Weld Made with Divergent Orifice, Same Parameters as Figures 2 and 3.

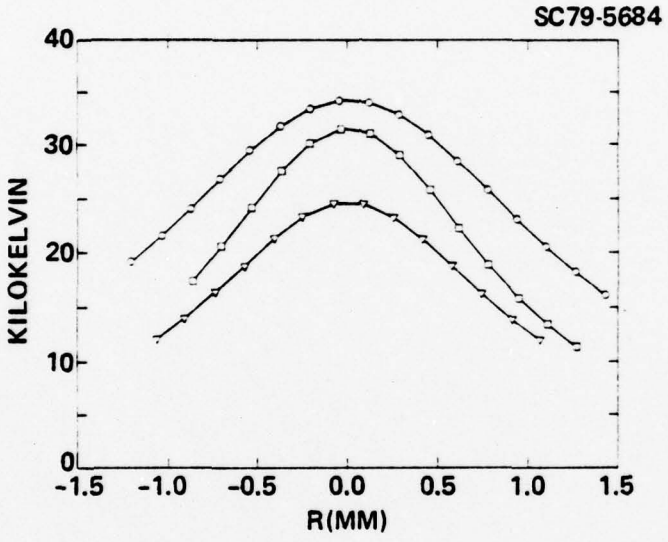

Fig. 1

APPENDIX C

DETERMINATION OF TEMPERATURE DISTRIBUTIONS IN WELDING PLASMAS

Rockwell International Science Center document SC-PP-79-74, submitted for publication in IEEE Transactions on Plasma Science

DETERMINATION OF TEMPERATURE DISTRIBUTIONS IN WELDING PLASMAS

C.B. Shaw, Jr.

Rockwell International Science Center

Thousand Oaks, California 91360

Abstract — The plasma diagnostic technique of two-directional monochromatic photography has been shown to permit time- and space-resolved measurement of temperature distributions in the unstable and asymmetric plasmas used in welding processes. The experimental and computational methods, first developed for study of the gas-tungsten arc welding process, have been subjected to a comprehensive sensitivity analysis, refined, and used in a study of the effects of orifice geometry on the performance of a torch used in the plasma-arc welding process. Representative temperature distributions are presented and compared with results obtained by other methods.

I. INTRODUCTION

The gas-tungsten arc welding (GTAW) process uses a short, high-pressure arc burning freely in a stream of inert gas such as

argon. One electrode, normally the anode, is the workpiece which is melted by the arc's conversion of electrical energy into thermal energy. The other electrode is a cylinder of tungsten, ground to a conical tip, which is immersed in the flowing argon. Arc pressure, neutral-gas stagnation pressure, the relative motion of cathode and anode, gravity, surface tension, and $j \times B$ forces drive the bulk circulation and complex surface oscillations of the molten portion of the anode, the weld pool. These motions change the boundary conditions of the arc and cause it to have a temperature distribution which is asymmetric and is rapidly time-varying in a way that reveals technologically significant information on operation of the welding process.[1-3] The plasma-arc welding (PAW) process resembles GTAW, but the tungsten electrode is surrounded by a copper orifice cup. The orifice may be a right circular cylinder, a convergent or divergent cone, or a combination of such shapes. The cup, its orifice, the tungsten cathode, and the axis of symmetry of argon streamlines are all coaxial. A small "pilot arc" current flows between cathode and cup to pre-ionize the argon stream, but because of a ballast resistor between cup and anode the major current path between cathode and anode is through the plasma which streams through the orifice towards the anode.

For some fraction of the "standoff" distance from orifice to workpiece, the plasma will be found to be very nearly symmetrical about the system axis of symmetry; that fraction depends primarily

on the travel speed of the torch relative to the workpiece. A complete study of the process, however, requires a diagnostic technique that can cope with substantial deviations from axial symmetry. The analytical and experimental requirements for this technique are discussed in the following two sections, followed by a discussion of results obtained by preliminary application of the technique.

II. THEORETICAL CONSIDERATIONS

Temperature T at any given point (r,θ,z) in a welding plasma can be calculated from the measured values of the local emission coefficients $f_i(r,\theta,z)$ for two spectral lines (i=1,2) of the same species, according to the formula[4]

$$T(r,\theta,z) = \frac{E_1 - E_2}{k \log [A_1 g_1 \lambda_2 f_2(r,\theta,z)/A_2 g_2 \lambda_1 f_1(r,\theta,z)]} . \qquad (1)$$

This follows from each emission coefficient being dependent on temperature according to

$$f_i = [bA_i g_i n(T)/u(T)\lambda_i] \exp (-E_i/kT) \qquad (2)$$

where n(T) and u(T) are the total particle density and partition function of the plasma, b and the Boltzmann constant k are universal

constants and, for each line, A_i is the Einstein spontaneous emission coefficient for the atomic transition producing wavelength λ_i, and g_i and E_i are the degeneracy and energy of the upper energy state from which the transition takes place. More accurate than the two-line method, Eq. (1), is the N-line method.[4] The latter is based on the fact that, according to Eq. (2), if the weighted emission φ_i, which is defined by

$$\varphi_i \equiv f_i\lambda_i/A_ig_i \tag{3}$$

is plotted against E_i, then the slope m of a straight-line fit to the data:

$$\log \varphi_i \sim a + mE_i \tag{4}$$

for i=1,2,···,N gives the temperature as

$$T = -1/km \ . \tag{5}$$

(In Eq. (1) the slope was evaluated analytically for N=2.)

Both the two-line method and the N-line method have the important advantage of not requiring even approximate values of quantities which are ill defined in an inhomogeneous plasma of

uncertain composition, such as a welding plasma. Other methods[4] all require n(T) and u(T) or other quantities which can only be computed (with some difficulty) for pure gases, uncontaminated by metal vapor from the workpiece. The importance of this limitation is illustrated by Fig. 1, which shows two microdensitometer scans of a spectrogram recorded by imaging the PAW plasma's nominal axis of symmetry onto the entrance slit of the spectrograph. The upper scan, which records the intensity of light coming from the plasma near the torch orifice, shows 16 identified lines of the Ar_{II} spectrum rising above the continuum radiation. The lower scan, which records the intensity of radiation originating near the mild-steel workpiece, shows those lines greatly weakened but adds 14 identified lines of the Mn_I and Fe_I spectra. The lines are those indicated in Table I.

The emission coefficients cannot be measured directly. Each must be inferred from the integrated intensity $I(x,\xi,z)$ projected onto a plane oriented parallel to the plane $\theta=\xi$. Since each integrated intensity is related to the corresponding local emission coefficient by

$$I_i(x,\xi,z) = \int_{-\infty}^{\infty} f_i(r,\theta,z)dy \tag{6}$$

with

$$x = r\cos(\theta-\xi) \quad , \quad y = r\sin(\theta-\xi) \tag{7}$$

coupled sets of equations, like Eq. (6), must be solved for all x and ξ and for each z and i, to obtain the $f_i(r,\theta,z)$. This is a generalization to systems without axial symmetry of the familiar Abel inversion problem.[4]

Olsen and his co-workers showed[5-7] that any quadratically-integrable function $f_i(r,\theta,z)$ can be represented almost everywhere by the series expansion

$$f_i(r,\theta,z) = \alpha\pi^{-\frac{1}{2}} \exp\,[-(\alpha r)^2] \sum_{m=0}^{\infty} \sum_{n=0}^{\infty} (-4)^n n!(2\alpha r)^m L_n^{(m)}[(\alpha r)^2] \times [C_i(m,n,\alpha,z) \cos\,(m\theta) + A_i(m,n,\alpha,z) \sin\,(m\theta)] \tag{8}$$

where the $L_n^{(m)}$ are *associated Laguerre polynomials*.[8] Substitution into Eq. (6) and evaluation of the integral shows that Eq. (8) implies

$$I_i(x,\xi,z) = \exp\,[-(\alpha x)^2] \sum_{m=0}^{\infty} \sum_{n=0}^{\infty} H_{m+2n}(\alpha x)[C_i(m,n,\alpha,z) \cos\,(m\xi) + A_i(m,n,\alpha,z) \sin\,(m\xi)] \tag{9}$$

with H_{m+2n} the Hermite polynomial of order m+2n.[8] They did not discuss the problem of choice or determination of the scale factor α, but showed that the sets of coefficients $\{C_i,A_i\}$ which appear in both Eqs. (8) and (9) could be determined from the experimental

data, the values of I_i, by use of the orthogonality relations satisfied by the trigonometric functions and the Hermite polynomials. However, this requires data acquisition for enough projection directions to permit numerical integration over ξ, as well as over x for each ξ. The procedure used in the present work reduced the onerous requirement of numerous projection directions (e.g., 37 views, every 5° from ξ=0° to ξ=180°[7]) to only two projections.[9] The scale factor α and the coefficients $\{C_i, A_i\}$ are determined iteratively from Eq. (9) for $\xi=\xi_0$ and for $\xi=-\xi_0$ which, for each choice of α, are treated as a set of simultaneous linear algebraic equations to be solved for $\{C_i, A_i\}$. The doubly-infinite series is of course truncated after a suitable number of terms. A satisfactory initial estimate of the scale factor, α_0, is obtained from a least-squares fit of the data to the ultimate truncation of Eq. (9), namely

$$I_i(x,\xi,z) \sim C_i(0,0,\alpha_0,z) \exp\left[-(\alpha_0 x)^2\right] \tag{10}$$

for each i and z and for both values of ξ. The iteration technique then generates a sequence $\{\alpha_p\}$ of approximations to α, and corresponding coefficients $\{C_i(m,n,\alpha_p,z),\ A_i(m,n,\alpha_p,z)\}$, in a way that optimizes—by a specific measure[9] — the precision with which the truncated series represents the experimental intensity data. The

final values of the scale factor and the coefficients can then be substituted into Eq. (8) to represent the local emissivities for each spectral line.

When the above procedure is used to solve Eq. (6) it still must be noted that Eq. (6) is not a "well-posed" problem. Hadamard[10] defined a well-posed problem as one for which the solution (i) exists, (ii) is unique, and (iii) depends continuously on the data — i.e., a small change in the data produces only small changes in the solution. Equation (6) satisfies none of these criteria. The data may be inconsistent, so that no exact solution exists. There may be oscillatory functions f_o (representing sinks as well as sources of radiation) which satisfy

$$0 = \int_{-\infty}^{\infty} f_o(r,\theta,z)dy \tag{11}$$

so that if f_i satisfies Eq. (6) so also does $f_i + af_o$ for any constant a. Likewise, there may be an oscillatory function f_ε, not necessarily of small amplitude, which satisfies

$$\varepsilon\delta(x-x_0,\ \xi-\xi_0) = \int_{-\infty}^{\infty} f_\varepsilon(r,\theta,z)dy \tag{12}$$

with ε small but non-zero, in which case the addition of ε to the measured intensity at a single point changes the solution of Eq. (6)

from f_i to $f_i + f_\varepsilon$. Because Eq. (6) is ill-posed, the solution procedure[9] does not attempt exact solution of the system of linear algebraic equations for the coefficients, but estimates their values by the method of best accessible estimation.[11] That method is stable against experimental error, avoids cumulative computational error, recognizes the existence of background and measurement error random processes, and replaces the ill-posed problem by its well-posed stochastic extension as suggested by Franklin.[12]

The entire solution procedure has been tested on simulated data for the same source, a displaced Gaussian, used by Olsen.[7] The absolute error was somewhat worse, but the relative error somewhat better, with the new procedure even though no more than 80 data points (40 on each of 2 projection planes) were used[8] instead of the 5957 data points (161 on each of 37 projections) used by Olsen.[7] Moreover, the error did not increase significantly when the simulated data were contaminated by pseudo-random background and measurement errors.

III. EXPERIMENTAL TECHNIQUES AND DATA REDUCTION

Intensity data were recorded by photographing the plasma as it appeared simultaneously from two view directions, $\xi = \pm 43.5°$, and at two wavelengths. As shown in Fig. 2, the experimental apparatus consisted of four major subsystems. An argon-filled inert atmosphere

box (I) held a stationary PAW torch and a rail-mounted translation stage which moved a water-cooled grooved copper backing bar, carrying the weld specimen, past the torch. View ports allowed arc radiation to enter the two-directional optical system (II) and the monochromator/spectrograph (IV). System II compressed the 87° angle between view directions to 3°, which could be handled by a single two-wavelength camera (III). The transfer lens (L) imaged each view of the plasma at plane P with unit magnification. The objective lens of the camera imaged plane P and the two plasma views at the center of the beamsplitter which divided the radiation into two paths. Each path contained an appropriate narrow-bandpass filter, F1 or F2, in front of a final lens which imaged the beamsplitter onto the film plane. The image-quality thin film interference filters, with bandwidth well under 1 nm, were centered on ionized argon lines in the visible spectrum or on neutral argon lines in the near infrared. A Compur type shutter Sh controlled exposure time. Another plasma image was also focused onto the input slit of a 0.3 m Czerny-Turner scanning monochromator, modified for spectrographic use (IV). Not shown in Fig. 2 is a Dove prism which could be used to rotate the image 90° about the optical axis of the system so that the input slit of the spectrograph could select radiation from a horizontal, rather than a vertical, section through the plasma. A micrometer drive, which moved the entire monochromator horizontally, could then be used to select the particular horizontal section of the plasma to be studied spectrographically.

All film was held and advanced by Exacta 35 mm camera bodies, and all three film strips were processed together to complete the data recording process. A Photometrics EDP Scanning Microscope, calibrated against a standard gray scale, was used to measure film density of the four arc images, spectrogram, and film-calibration exposures made with a stable light source and neutral-density filters.

The spectrograph did not provide sufficient data to permit accurate point-by-point subtraction of continuum intensity from the intensity of continuum plus Ar_{II} lines, but the wavelengths of the Ar_{I} lines are free of any continuum and could be used to study asymmetric plasmas. A typical isotherm pattern, measured in the horizontal plane 1.0 mm below the torch orifice, is shown in Fig. 3. The data were recorded during welding of a titanium alloy (Ti-6Aℓ-4V) at 70 amperes. The workpiece moved in the 0° direction at 4 inches per minute. Note that the temperature gradient is much greater in the vicinity of 180°, where cold metal is moving in under the torch, than at 0° where the hot weld puddle and the hot, newly-completed, weld moves away from the torch. The asymmetric height of circulating weld puddle molten metal (some 5 mm below the reference plane of the figure and about 6 mm in diameter) has displaced the point of maximum temperature approximately 1 mm from the symmetry axis of the torch.

For certain combinations of welding parameters, the plasma radiation intensity did show good axial symmetry for a certain

limited distance below the torch orifice. The spectrograph, with the Dove prism in place, could then provide sufficient data (for one horizontal plane at a time) for conventional Abel inversion. This meant that four Ar_{II} lines, corrected for continuum intensity, could be used for temperature measurement by the N-line method. Figure 4 shows typical results obtained in this way. Temperature is displayed as a function of radius in each of four horizontal planes.

A number of side experiments were conducted to evaluate the sensitivity of temperatures measured by these methods to the following factors: (1) dependence of center-wavelength and bandwidth of the narrow-band filters on angle of incidence of the light, (2) differences in transmittance across the face of the filter, (3) the possibility of self-absorption by the plasma of its emitted spectral lines, (4) deviation of the photographic film exposure curve from its nominal value, and (5) errors in the published values of the quantum mechanical quantities, primarily A_i, appearing in Eq. (3). It was found that even the 3° residual angle between apparent view directions (produced by subystem II in Fig. 2) was enough to allow one or the other view direction to reach a portion of the transmittance versus angle of incidence curve which is rapidly varying. This means that extreme care had to be exercised to place the optical axis of the camera exactly midway between the two view directions. In future,

separate multiwavelength cameras will be used for each view direction to avoid this problem. Scanning of the filter surfaces showed that variations in transmission could have been a severe problem had the filters been placed near a focal plane; however, this was avoided by mounting them at a transfer lens. By use of an auxiliary mirror, which could be placed behind the plasma, and by dilution of the argon with helium, evidence was accumulated against self-absorption at the wavelengths of interest. Because of the size and shape of the plasma, the radiated intensity observed at each point does not double when the mirror is put in place, but the actual ratio (roughly 1.6) is independent of the percentage of argon in the gas over more than a decade. The photographic film exposure curve did appear to deviate from its nominal value, even from frame to frame, but, as is discussed below, this could be corrected by regression analysis. Another statistical analysis indicates errors in the A_i for the Ar_{II} lines, which have thus been corrected.[13]

In many cases where, because of symmetry, the spectrographic data alone were adequate for temperature measurement, it was found that the intensity data were well fitted by a simple Gaussian, provided that the origin was slightly shifted along the line of welding by an amount which increased with increasing vertical distance below the orifice. The intensity of Ar_{II} lines, as obtained from the calibrated microdensitometer readings and the film calibration

curve (density versus log intensity), was corrected by subtraction of the average continuum intensity on either side of the line. These raw values of log intensity were then smoothed, as functions of horizontal position x, by replacing each value by the median of itself and the values at the two neighboring values of x. (End-point data were replicated for this purpose.) This smoothing by moving medians of three was iterated to convergence. The smoothed data were fitted to the Gaussian form by iteratively weighted linear least squares, and the residuals in log intensity after the final iteration, namely

$$e_{ij} \equiv \log (I_{ij}) - \log (\hat{I}_{ij}) \ , \tag{13}$$

were analyzed by guided regression[14] to see if there was a systematic error in I_{ij}, dependent on the density d_{ij}, due to an error in film calibration. The customary F-statistic was used to test the null hypothesis that the apparent goodness of fit of the residuals to a selected set of functions of d_{ij} was the result of sampling independent random processes. The hypothesis was always rejected far beyond the 99.9% confidence level, the highest tabulated.[15] Improvement in the confidence level was used to determine whether additional functions of density were needed to fit e_{ij}, or if one should be dropped from the present set. Since it is foolhardy to follow any

fixed rule in regression analysis without checking to see if the results are reasonable,[14] graphic comparison was made between the nominal film calibration curve and the curve as corrected by the regression analysis. The results of the regression analysis were rejected on this basis in a few cases, which proved to be those in which the data deviated the most from the assumed simple Gaussian form.

Where possible, then, regression analysis corrected the intensities for systematic errors stemming from the film calibration, and local emissivities were calculated from the intensities by Abel inversion. The inversion is trivial in these cases, where the experimental data are adequately described by Eq. (10), since then from Eq. (8) or directly from Eq. (6) one has simply

$$f(r,\theta,z) = \alpha\pi^{-\frac{1}{2}}C_i(0,0,\alpha_0,z)\ \exp\ [-(\alpha_0 r)^2]\ . \tag{14}$$

For each x_j, ordinary least-squares fitting of the weighted log emissivity to E_i gave the temperature T_j, according to Eqs. (3-5). The residuals from this fitting,

$$r_{ij} \equiv \log\ \varphi_{ij} - (a+mE_i)\ , \tag{15}$$

were also studied and showed a very consistent pattern: the scatter of log (φ_{ij}) about the fitted line was virtually unchanged, for one

value of x_j after another, in test after test. These persistent residuals were attributed to errors in the published values[16] of A_i. A test based on Student's t[17] strongly rejects the null hypothesis that the observed residuals were samples from a population of zero mean. The confidence level at which the null hypothesis was rejected, and the corrected value of A_i for the Ar_{II} lines at wavelengths 476.489, 480.607, 484.790, and 487.990 nm, are given elsewhere.[13]

IV. DISCUSSION

The measured temperatures, such as shown in Figs. 3 and 4, range about twice as high as those recently reported by Quigley and co-workers,[18] who used Langmuir probes to measure PAW plasma temperature. This discrepancy may be due to perturbation of the plasma by their probes, or to residual error in our data. Glickstein's measurements[19] could be consistent either with our values or with Quigley's; in the absence of any regression analysis, his error bars are comparable to the full range of temperatures measured. The values reported by Mills,[20] all less than 5000°K, were all measured close to the workpiece where the temperature no doubt is much lower than in the region, closer to the torch, where our measurements were made. However, following Ludwig,[21] Mills used the one-line method[4] to measure temperature via emission from

metal vaporized into the plasma from the workpiece. This method, although appealing in its simplicity, requires knowledge of T^*, the temperature at which emission of the observed line is a maximum. Because of the impurity and uncertain composition of a welding plasma, T^* could be a source of gross inaccuracy. It should be noted that Quigley, Glickstein, Mills, and Ludwig all assumed axial symmetry for the plasmas they measured. Only Olsen's group[6,7,22] undertook to resolve asymmetric temperature distributions, as (in part) was done here, and that was done at the price of gathering so much experimental data that measurements could not be made on an actual welding arc, but only on an artificially-stabilized arc burning over a water-cooled copper anode. Each experiment required eight hours to perform[22] in sharp contrast to the experiments reported here, in which all data were recorded at snapshot speed.

A striking feature of Fig. 4 is that the temperature curve for the lowest level crosses the other three curves. This means that heat flows downward, towards the workpiece, in the central region of the plasma as expected, but at least the conductive component of heat flow is upwards outside the central region. This confirms evidence previously obtained by holographic interferometry[1] that some heat indeed flows down into the workpiece but then quickly flows out through the workpiece and back into the gas. The crossing over of temperature curves was also observed by Quigley.[18]

The technological implications of these temperature measurements are reported elsewhere.[23] Future applications of these measurement techniques will, as previously indicated, use separate cameras for each view direction. This will permit all optical components to be squared to the optical axis for minimum aberrations. In view of the analysis of residuals reported here, future applications will use four spectral lines, rather than two, as was first attempted.[2] By use of multiple beam splitters, separate images will be recorded for each spectral line and for any continuum samples required. The practicability of using charge-coupled device arrays to replace the troublesome photographic film will be investigated.

V. ACKNOWLEDGEMENTS

This work was supported in part by Rockwell International under its Independent Research and Development Program, and in part by the U.S. Navy, Office of Naval Research, Project 471, under contract N00014-75-C-0789. The author is deeply grateful to B.I. Davis, without whose dedication and ingenuity the experiments would have been impossible, and thanks D.W. Trover for assistance both in the laboratory and with data reduction. Much benefit and stimulation was derived from discussions with S.S. Glickstein, G.S. Mills, H.N. Olsen, J.F. Key, and T.W. Eagar.

A preliminary version of this paper was presented at the annual meeting of the Plasma Physics Division of the American Physical Society, 30 October – 3 November 1978, Colorado Springs, Colorado.

REFERENCES

[1] C.B. Shaw, Jr. and B.I. Davis, "Diagnostic Arc Studies with Ruby Laser," in Developments in Laser Technology – II Proc. Soc. Photo-Opt. Inst. Eng. 41, 89-99 (1973).

[2] C.B. Shaw, Jr. and B.I. Davis, "Time-Resolved Temperature and Density Distributions in a Welding Arc," IEEE Conference Record First Int'l. Conf. on Plasma Science 74CH0922-5-NPS, p. 13 (1974).

[3] C.B. Shaw, Jr., "Diagnostic Studies in GTAW Arc. Part 1 – Observational Studies. Part 2 – Mathematical Model," Welding J. 54 (2) 33s-44s, 54 (3) 81s-86s (1975).

[4] W. Lochte-Holtgreven, "Evaluation of Plasma Parameters," in W. Lochte-Holtgreven, ed. Plasma Diagnostics, Ch. 3, John Wiley & Sons, New York (1968).

[5] C.D. Maldonado, "Note on Orthogonal Polynomials Which Are 'Invariant in Form' to Rotation of Axes," J. Math. Phys. 6, 1935-1938 (1965).

[6] C.D. Maldonado and H.N. Olsen, "New Method for Obtaining Emission Coefficients from Emitted Spectral Intensities. Part II – Asymmetrical Sources," J. Opt. Soc. Am. 56, 1305-1313 (1966).

[7] H.N. Olsen, C.D. Maldonado, and G.D. Duckworth, "A Numerical Method for Obtaining Internal Emission Coefficients from Externally Measured Spectral Intensities of Asymmetrical Plasmas," J. Quant. Spectrosc. Radiat. Transfer 8, 1419-1430 (1968).

[8] Gabor Szegö, Orthogonal Polynomials, Colloquium Publications Vol. XXIII, American Mathematical Society, Providence, Rhode Island, Ch. V (1939).

[9] C.B. Shaw, Jr., "Reconstruction of Certain Distributions from Very Limited Projection Data," Rockwell International Science Center preprint SC-PP-79-75, submitted for publication in SIAM J. Num. Anal. (1979).

[10] J. Hadamard, Lectures on Cauchy's Problem in Linear Partial Differential Equations, Dover, New York (1952).

[11] C.B. Shaw, Jr., "Best Accessible Estimation: Convergence Properties and Limiting Forms of the Direct and Reduced Versions," J. Math. Anal. Appl. 44, 531-552 (1973).

[12] Joel N. Franklin, "Well Posed Stochastic Extensions of Ill Posed Linear Problems," J. Math. Anal. Appl. 31, 682-716 (1970).

[13] C.B. Shaw, Jr., "Statistical Inference of Four Ar_{II} Transition Probabilities," Rockwell International Science Center preprint SC-PP-79-72, submitted for publication as a Note in J. Quant. Spectrosc. Radiat. Transfer (1979).

[14] Frederick Mosteller and John N. Tukey, Data Analysis and Regression, Reading, Massachusetts, Addison-Wesley (1977).

[15] Milton Abramowitz and Irene A. Stegun, eds., Handbook of Mathematical Functions, Ch. 26, Washington, D.C., National Bureau of Standards (1964).

[16] Rudolph Schapouff, "Über Messungen von A_{II} Übergangswahrscheinlichkeiten und die Kontinua von A und Ne," Z. Astrophys. 68, 431-444 (1968).

[17] John F. Kenney, Mathematics of Statistics, Part Two, Ch. VII, D. Van Nostrand Company, New York (1941).

[18] C.J. Allan, J.C. Metcalfe, and M.B.C. Quigley, "A Modified Low Pressure Probe Theory Applied to the Measurement of Temperature Profiles in Plasma-Welding Arcs," International Institute of Welding Document 212/396/77, Central Electricity Generating Board (1977).

[19] S.S. Glickstein, "Temperature Measurements in a Free-Burning Arc," Westinghouse Bettis Laboratory, Report WAPD-TM-1216 (September 1975).

[20] G.S. Mills, "Use of Emission Spectroscopy for Welding Arc Analysis," Welding J. 56, 93s-96s (1977).

[21] H.C. Ludwig, "The Measurement of Temperature in Welding Arcs," Electrical Engineering 79, 565-569 (1960).

[22] H.N. Olsen, private communication (1971).

[23] C.B. Shaw, Jr., "Effect of Orifice Geometry in Plasma-Arc Welding of Ti-6Aℓ-4V," Rockwell International Science Center preprint SC-PP-79-73, submitted for publication in Met. Trans. (1979).

CAPTIONS

Table I. Wavelengths versus Identification Numbers Shown in Fig. 1

Fig. 1. Microdensitometer Scans of Spectrogram of Welding Plasma. Top: Above Midplane. Bottom: Near Workpiece. Lines Identified in Table I.

Fig. 2. Schematic Diagram of the Experimental Apparatus.

Fig. 3. Isothermal Contours 3,000°K to 25,000°K During Plasma-Arc Welding of Titanium at 70 A, 4 ipm, 1.0 mm Below Torch Orifice.

Fig. 4. Temperature Measured in Four Horizontal Planes Below the Torch: X 0.67 mm ○ 1.00 mm □ 1.33 mm o 1.67 mm.

I.D. Number	Wavelength (nm)	Species
1	463.723	Ar II
2	465.789	"
3	472.686	"
4	473.591	"
5	476.486	"
6	480.602	"
7	484.782	"
8	486.592	"
9	487.986	"
10	488.903	"
11	490.475	"
12	493.321	"
13	496.507	"
14	500.933	"
15	501.716	"
16	506.204	"
17	470.972	Mn I
18	473.911	"
19	475.404	"
20	476.153	"
21	476.238	"
22	476.586	"
23	476.643	"
24	478.342	"
25	482.352	"
26	487.133	Fe I
27	489.150	"
28	492.051	"
29	495.761	"
30	504.176	"

SC79-4964

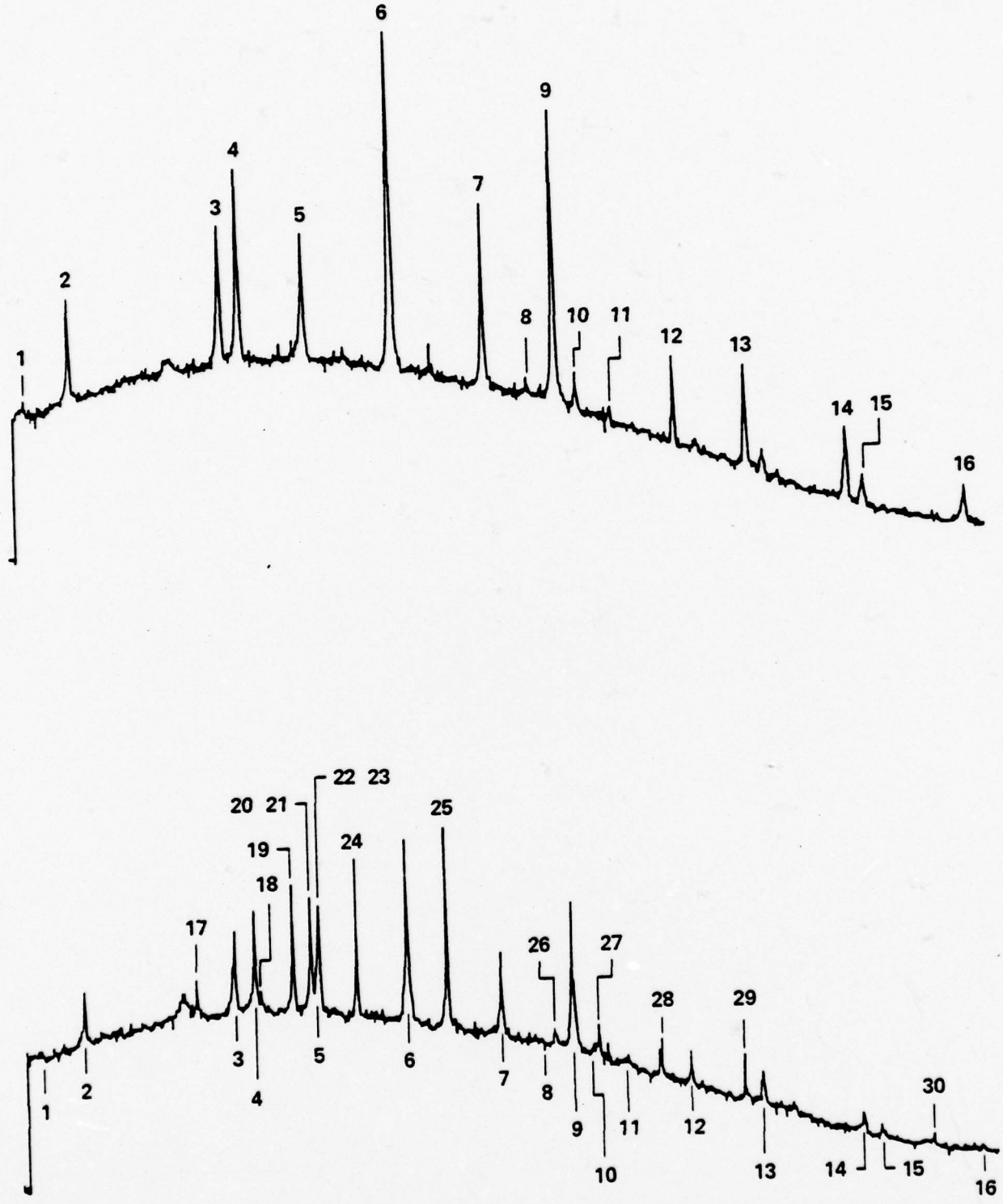

Fig. 1

SC79-4961

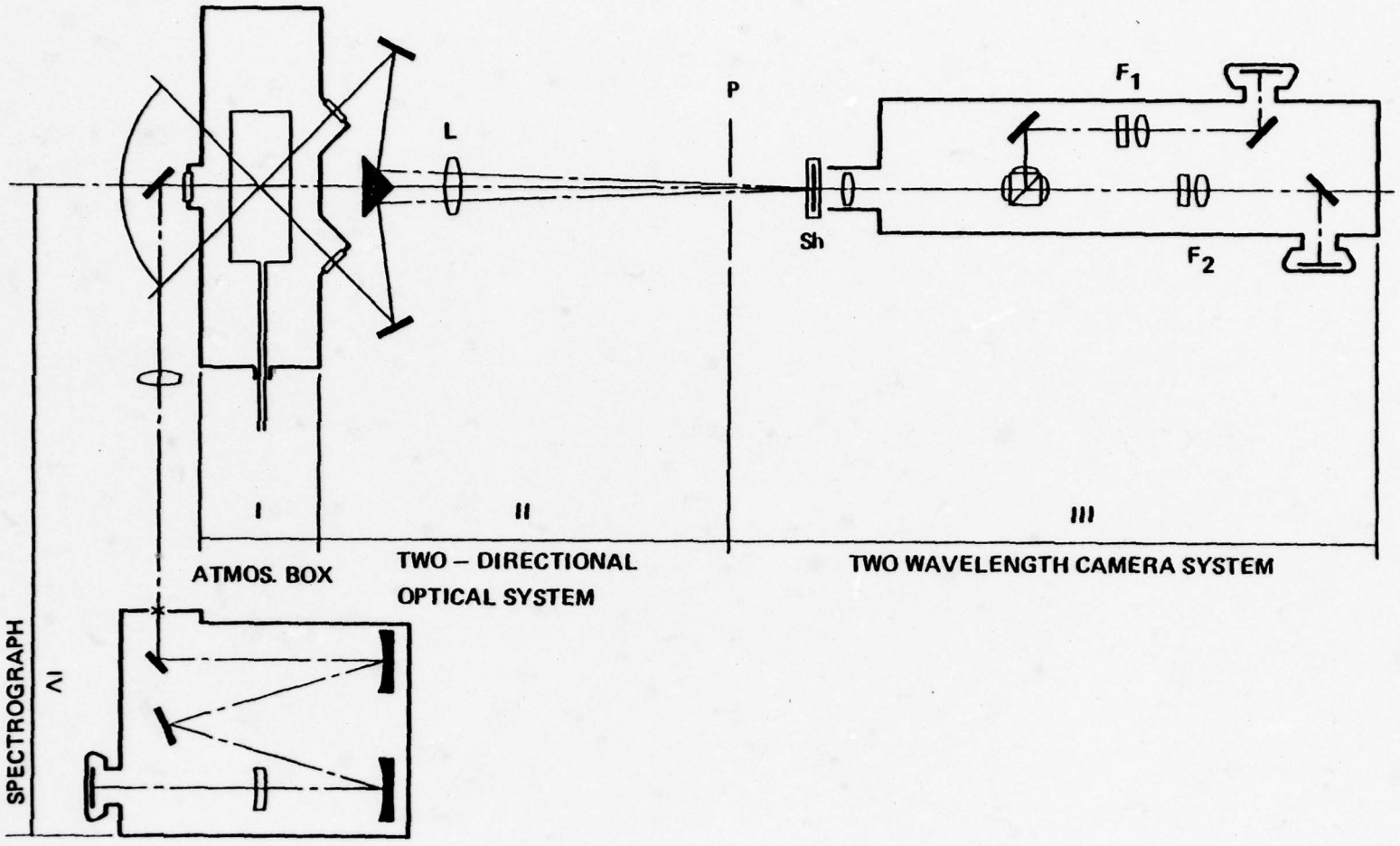

Fig. 2

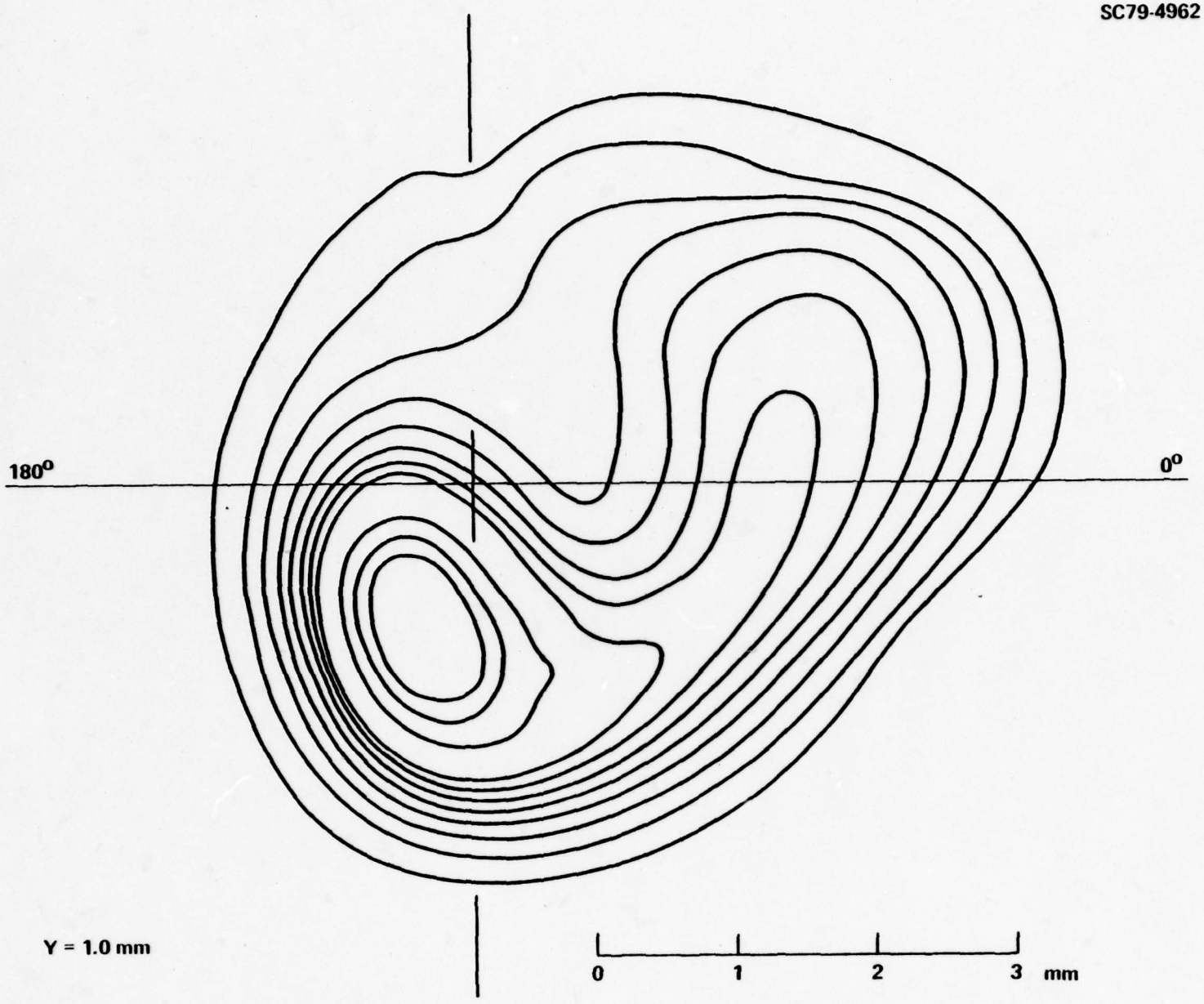

Fig. 3

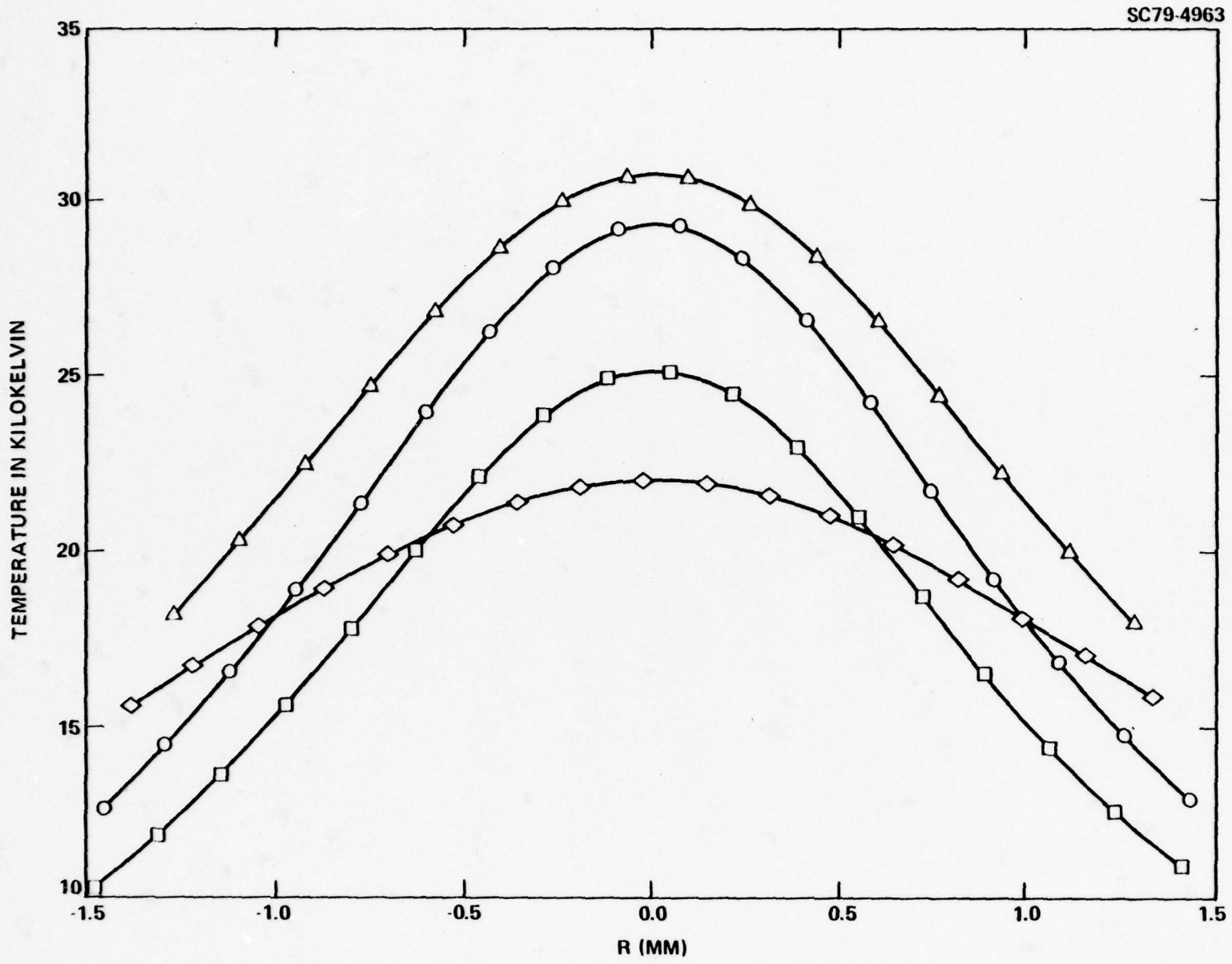
SC79-4963
TEMPERATURE IN KILOKELVIN
35
30
25
20
15
10
-1.5
-1.0
-0.5
0.0
0.5
1.0
1.5
R (MM)

Fig. 4

APPENDIX D

RECONSTRUCTION OF CERTAIN DISTRIBUTIONS FROM VERY LIMITED PROJECTION DATA

Rockwell International Science Center document SC-PP-79-75, submitted for publication in SIAM J. Num. Anal.

ABSTRACT

The problem addressed is determination of a function, given integrals of the function along variously spaced and directed lines. No special symmetry is assumed. The basis-function method, most useful when the data indicates a roughly Gaussian or exponential behavior, is improved by eliminating the need for pre-knowledge of a special scale factor, and by greatly reducing the necessary number of data points. A solution algorithm is presented which limits accumulation of computational error and is stable in the presence of experimental errors. Comparisons are made with exact analytical results and with the results of an older method.

RECONSTRUCTION OF CERTAIN DISTRIBUTIONS FROM VERY LIMITED PROJECTION DATA

1. Introduction

The problem of reconstructing functions in three dimensional space from their projections, or line integrals along various directions, dates from the discovery of x-rays. It is found in such apparently unrelated fields as radio astronomy, nuclear medicine, electron microscopy, holographic interferometry, and plasma physics. Computational methods for this generalization of Abel inversion to non-axisymmetric systems therefore tend to be discovered and rediscovered, without knowledge of prior work published in the specialized literature of another application area. Marr [5] and Gordon [2] have organized broadly interdisciplinary workshops to expose the areas of commonality among the various applications. Significant areas of difference also exist, however. For example, if the function to be reconstructed represents tissue density, an important medical requirement is accurate detection of variation by a few percent in a region (representing a cancerous lesion) quite small compared to the whole region examined, despite the existence of jump discontinuities by a factor of two at the boundary between soft tissue and bone. An opposite extreme is presented by plasma diagnostics, where the unknown function may represent the emission coefficient for radiation in a certain

wavelength interval. This quantity may vary by several orders of magnitude over a region of interest which has no sharply-defined boundaries, but the variation is fairly smooth and relatively uncomplicated even when the data represents significant technological information. Algorithms developed to solve the medical problem typically require data on the results of irradiating the patient 180 times, at increments of one degree in azimuth. We shall see that two projections suffice for the plasma-diagnostic type of problem, even though many more had previously been used by Olsen [6] and his co-workers, whose basis-function method we have extended. Pre-knowledge of a scale factor for spatial variation of the emission coefficient is no longer required, the deleterious effects of unavoidable experimental error have been minimized, and much less experimental data is necessary than previously realized.

2. Basis-Function Method

The problem is to solve a set of linear integral equations of the first kind,

$$\int_{-\infty}^{\infty} f(r,\theta,z)dy = g(x,\xi,z) \qquad (1)$$

for the unknown source function $f(r,\theta,z)$, given intensity data g measured at various levels z for projections recorded at various

orientation angles ξ. Each value of z poses a separate problem, uncoupled to the others, but for each z the data for all values of ξ must be utilized. We shall shortly drop z from the notation. The cylindrical coordinates (r,θ,z) are defined relative to a fixed laboratory frame of reference, while the Cartesian coordinates (x,y,z) are re-defined for each projection: y, the normal to the projection plane, is equivalently the direction of projection, z is as in the laboratory frame, and x the orthogonal axis in the projection plane. The coordinate systems are related by[1]

$$x = r \cos(\theta-\xi) \quad , \quad y = r \sin(\theta-\xi) \; . \tag{2}$$

Olsen's method for solving Eq. (1) was to expand $f(r,\theta)$ in terms of trigonometric functions of θ and associated Laguerre

---

[1]There is an unfortunate inconsistency in the definition of the sign of ξ in Olsen [6] carried over from Maldonado and Olsen [4]. The figures in [6] and [4] show the angle ξ, between θ=0 and the x-axis, taken positive in the same sense as θ, as is done here. The text of [6] and [4] implies that positive ξ was defined in the opposite way, from the positive x-axis to θ=0, but we have verified that the analysis was actually consistent with our Eq. (2).

polynomials $L_k^{(n)}(\alpha^2 r^2)$, multiplied by, essentially, the weight function with respect to which the $L_k^{(n)}$ are orthogonal on the interval $[0,\infty)$. That is,

$$f(r,\theta) = \alpha\pi^{-\frac{1}{2}} \sum_{k=0}^{\infty} \sum_{n=0}^{\infty} (-4)^k k!(2\alpha r)^n L_k^{(n)}(\alpha^2 r^2) e^{-\alpha^2 r^2} [B(n,k,\alpha) \cos n\theta + D(n,k,\alpha) \sin n\theta] \ . \quad (3)$$

Substitution of Eq. (3) into Eq. (1) and use of Eq. (2) gives [4]

$$g(x,\xi) = \sum_{k=0}^{\infty} \sum_{n=0}^{\infty} e^{-\alpha^2 x^2} H_{n+2k}(\alpha x)[B(n,k,\alpha) \cos n\xi + D(n,k,\alpha) \sin n\xi] \quad (4)$$

where the Hermite polynomials H emerge as basis functions for representation of g. (We have renormalized the coefficients somewhat to simplify Eq. (4).) The coefficients $\{B,D\}$ can then in principle be obtained from experimental values of $\{g(x,\xi)\}$ since, by virtue of the orthogonality relations

$$\int_{-\infty}^{\infty} H_m(u) H_n(u) e^{-u^2} du = \delta_{nm} \sqrt{\pi} 2^n n! \quad (5)$$

and

$$\int_{-\pi}^{\pi} \begin{matrix} \cos \\ \sin \end{matrix} m\theta \begin{matrix} \cos \\ \sin \end{matrix} n\theta d\theta = \delta_{nm}(1 + \delta_{n0})\pi \ , \quad (6)$$

$$\int_{-\pi}^{\pi} \begin{matrix} \cos \\ \sin \end{matrix} m\theta \begin{matrix} \sin \\ \cos \end{matrix} n\theta d\theta = 0 \ .$$

Eq. (4) implies

$$B(n,k,\alpha) = [\alpha\pi^{-3/2}2^{-(n+2k)}/(1 + \delta_{n0})(n + 2k)!]$$

$$\int_{-\pi}^{\pi}\int_{-\infty}^{\infty} g(x,\xi)H_{n+2k}(\alpha x)\cos n\xi dx d\xi \qquad (7)$$

and $D(n,k,\alpha)$ is given by the same double integral with cos $n\xi$ replaced by sin $n\xi$. Olsen accepted the necessity of obtaining enough data $\{g(x,\xi)\}$ to permit accurate numerical quadrature over ξ. No mention was made of how the scale factor α was to be determined.

Far less experimental data is required to compute $f(r,\theta)$ if one treats Eq. (4), for all x and ξ, as a set of simultaneous linear equations from which to estimate α and $\{B,D\}$. While it is well known that the sets of basis functions in Eqs. (3,4) are complete (see, e.g., Szegö [10]), so that any quadratically integrable function can be represented by the infinite series almost everywhere, the most practical application of the method arises in those cases where a very small number of terms in the series represents $\{g(x,\xi)\}$ with satisfactory accuracy. Economization of the truncated-series representation is achieved by proper choice of the scale factor, α.

The specific basis functions shown in Eqs. (3,4) were chosen on empirical grounds related to a specific application area. In

plasma diagnostic studies of freely-burning high pressure arcs the desired emission coefficients can be expected on physical grounds to exhibit nearly Gaussian dependence on r, with modest asymmetry. The r-dependence is therefore fitted to a Gaussian times polynomials which are orthogonal with the Gaussian as a weight function. Very close to the arc cathode the dependence on r should look more like exponential decay. Maldonado [3] has derived by a Gram-Schmidt process the basis functions appropriate to that case. Again they involve associated Laguerre polynomials, but in r rather than r^2, which are orthogonal with exp (-r) as weight function. Maldonado [3] asserts that the procedure can be used for other weight functions K(r) with respect to which polynomials $Q_n^m(r)$ are orthogonal on $[0,\infty)$. If the unknown function $f(r)$ is known or believed to behave like $K(\alpha r)$, one represents it more accurately by a series like that in Eq. (3), but with exp $(-\alpha^2 r^2)$ replaced by $K(\alpha r)$ and $(2\alpha r)^n L_k^{(n)}(\alpha^2 r^2)$ replaced by $Q_n^m(\alpha r)$. Substitution into Eq. (1) and evaluation of the integral by use of Eq. (2) then yields the series representation, equivalent to Eq. (4), to be fitted to the experimental data.

3. A Solution Algorithm

Equation (1) is not a well posed problem, by Hadamard's definition. Consequently, the computational scheme employed to solve Eq. (4) must be chosen carefully. A method which has been

employed successfully by Shaw, et al. [9] on experimental plasma diagnostic data is the following. The series in Eq. (4) is truncated, $n \leq N$, $k \leq K$. (The choice of N reflects the complexity of dependence of the data on orientation angle ξ for each projection, and limits the azimuthal variability which will be attributed to $f(r,\theta)$. The maximum degree of the polynomials fitted to the data and attributed to f is N+2K.) While in principle one can solve the resulting equation explicitly for α and the $(2N+1)(K+1)$ coefficients by nonlinear least squares, it is more practical to define a loss function and select a value for α, solve the linear (unweighted) least-squares problem for the coefficients, compute the loss function for the current value of α, and then iterate, using a sequence of values of α selected so as to minimize the loss function.

A starting value for α can be obtained by ultimate truncation of the series to n = k = 0, that is, the crude approximation

$$g(x,\xi) \simeq B(0,0,\alpha_1)e^{-\alpha_1^2 x^2} \quad . \tag{8}$$

The unweighted least-squares estimate α_1 is therefore

$$\alpha_1 = \left[\frac{\langle x^2\rangle\langle \log g\rangle - \langle x^2 \log g\rangle}{\langle x^4\rangle - (\langle x^2\rangle)^2}\right]^{\frac{1}{2}} \tag{9}$$

where $\langle\cdot\rangle$ is the average over all x for all ξ (and each z).

Also

$$B(0,0,\alpha_1) = \exp\left[\frac{\langle \log g\rangle\langle x^4\rangle - \langle x^2\rangle\langle x^2 \log g\rangle}{\langle x^4\rangle - (\langle x^2\rangle)}\right] \tag{10}$$

Even with this fixed value of α_1 the linear system of truncated Eq. (4) is described by a matrix which in general is ill-conditioned. One generally works with many more data points than unknowns, but the equations prove inconsistent, rather than overdetermined, due to experimental errors in the data. To avoid multiplying this error level by the large conditioning number, as in direct solution (in the least squares sense) of the overdetermined system, the method of best accessible estimation was developed by Shaw [7,8]. It is stable against experimental error, recognizes the existence of background and measurement-error random processes, and replaces the ill-posed problem by its well-posed stochastic extension, as suggested by Franklin [1]. It is an iterative procedure which, in the absence of computational error, would converge to the minimum residue estimate of minimum length for the solution to the problem, when residue and length are measured in the ellipsoidal norms defined by the autocorrelation operator for the measurement and background random error processes. The norm of the difference of successive estimates is monitored, and iteration stops when it signals the onset of excessive accumulated computational error. The

starting estimate, required to begin the iteration procedure, is that $B(0,0,\alpha_1)$ is given by Eq. (10) and all other coefficients are zero if the initial estimate, Eq. (9), is being used. When the p^{th} estimate of α, α_p, is being used one takes the best accessible estimate $\{B(n,k,\alpha_{p-1}), D(n,k,\alpha_{p-1})\}$ as the starting estimate of $\{B(n,k,\alpha_p), D(n,k,\alpha_p)\}$.

The loss function which drives iteration on α can be defined in terms of the residue and length, for the best accessible estimate at step p in α-iteration, by

$$L_p \equiv \|r_p\|^2_{R_{22}} \quad \|C_p\|^2_{R_{11}} \tag{11}$$

where the ellipsoidal norms are

$$\|u\|^2_R = u^* R^{-1} u \tag{12}$$

and R is the autocorrelation matrix of errors in the space in which u is a column vector. Here the column vector r_p has an element (r_p) for each x and ξ which is defined by

$$(r_p) \equiv g(x,\xi) - e^{-\alpha_p^2 x^2} \sum_{k=0}^{K} \sum_{n=0}^{N} H_{n+2k}(\alpha x)[B(n,k,\alpha_p) \cos n\xi + D(n,k,\alpha_p) \sin n\xi] \tag{13}$$

and R_{22} characterizes random errors in measurement of $g(x,\xi)$. By C_p in Eq. (11) is meant a single column vector whose elements are all the coefficients $B(n,k,\alpha_p)$ and $D(n,k,\alpha_p)$. The error autocorrelation matrix R_{11} for the space of C is related to that for background errors — random fluctuations superimposed on $f(r,\theta)$ — by Eq. (3). According to Eq. (6) and the orthogonality relation

$$\int_0^\infty L_k^{(\alpha)}(u)L_q^{(\alpha)}(u)e^{-u}u^\alpha du = \delta_{pq}\frac{(k+\alpha)!}{p!} . \tag{14}$$

Equation (3) implies

$$B(n,k,\alpha) = \frac{\alpha^{n-1}(-1)^k}{\pi^{\frac{1}{2}}(n+k)!(1+\delta_{n0})2^{n+2k}}\int_0^\infty\int_{-\pi}^{\pi} f(r,\theta)r^{n+1}L_k^{(n)}(\alpha^2r^2)\cos n\theta d\theta dr \tag{15}$$

and $D(n,k,\alpha)$ is given by the same expression with $n\theta$ in Eq. (15) replaced by $\sin n\theta$. In terms of the previously-defined vector C, Eq. (15) and its counterpart for D explicitly define the operator A in the expression

$$C = Af . \tag{16}$$

But if we call the autocorrelation operator for the background fluctuations R_{00}, Eq. (16) means that

$$R_{11} = AR_{00}A^* . \tag{17}$$

For example, if the background fluctuations are uncorrelated from point $\underline{r}$ to point $\underline{r}'$ and of uniform intensity in unit volume, then R_{00} in terms of a delta-function of position vectors is

$$R_{00} = \sigma^2 \delta(\underline{r}-\underline{r}') \tag{18}$$

which, with Eq. (17), means that R_{11} is also diagonal, that the element for $B(n,k,\alpha_p)$ or $D(n,k,\alpha_p)$ is

$$(R_{11}) = \frac{\sigma^2}{\alpha_p^4(1+\delta_{n0})(n+k)!k!2^{2n+4k+1}} \tag{19}$$

and that the length of the solution at step p is given by

$$\|C_p\|^2_{R_{11}} = \sum_{n=0}^{N} \sum_{k=0}^{K} \alpha_p^4(1+\delta_{n0})(n+k)!k!2^{2n+4k+1} \frac{[B^2(n,k,\alpha_p) + D^2(n,k,\alpha_p)]}{\sigma^2} \tag{20}$$

Measurement of length in the ellipsoidal norm frees it from dependence on the particular normalization of the coefficients, as they were defined in Eq. (3).

The specific form of the loss function shown in Eq. (11) stems from the fact that for any α_p best accessible estimation converges (in the absence of significant computational error) to that C_p which, among all that minimize $\|r_p\|^2_{R_{22}}$, also minimizes $\|C_p\|^2_{R_{11}}$, and therefore

minimizes their product. The purpose of choosing a new α_p is to make the minimum product even smaller. Standard numerical methods have been used for selection of α_{p+1}, given α_p, and L_p, for $p' = p, p-1, \cdots$ to find that $\{\alpha_p\}$ for which $\{L_p\}$ approaches a minimum.

It should be noted that, whenever the appropriate experimental data is available, computer core requirements can be reduced by a factor of 4 and run time by a factor of 4 to 16 (depending on the linear algebraic system-solving routine used) if the problem is first block-diagonalized. This is done by grouping the data into combinations which are symmetric and antisymmetric both in x and in ξ. If one defines

$$g_{ee}(x,\xi) \equiv \frac{1}{4}[g(x,\xi) + g(-x,\xi) + g(x,-\xi) + g(-x,-\xi)]$$

$$g_{eo}(x,\xi) \equiv \frac{1}{4}[g(x,\xi) + g(-x,\xi) - g(x,-\xi) - g(-x,-\xi)] \qquad (21)$$

$$g_{oe}(x,\xi) \equiv \frac{1}{4}[g(x,\xi) - g(-x,\xi) + g(x,-\xi) - g(-x,-\xi)]$$

$$g_{oo}(x,\xi) \equiv \frac{1}{4}[g(x,\xi) - g(-x,\xi) - g(x,-\xi) + g(-x,-\xi)]$$

then solution of the truncated version of Eq. (4) is reduced to solution of the four uncoupled sets of equations

$$g_{ee}(x,\xi) = e^{-\alpha^2 x^2} \sum_{k=0}^{K} \sum_{n=0}^{[N/2]} H_{2(n+k)}(\alpha x) B(2n,k,\alpha) \cos 2n\xi$$

$$g_{eo}(x,\xi) = e^{-\alpha^2 x^2} \sum_{k=0}^{K} \sum_{n=1}^{[N/2]} H_{2(n+k)}(\alpha x) D(2n,k,\alpha) \sin 2n\xi$$

(22)

$$g_{oe}(x,\xi) = e^{-\alpha^2 x^2} \sum_{k=0}^{K} \sum_{n=0}^{[(N-1)/2]} H_{1+2(n+k)}(\alpha x) B(2n+1,k,\alpha) \cos (2n+1)\xi$$

$$g_{oo}(x,\xi) = e^{-\alpha^2 x^2} \sum_{k=0}^{K} \sum_{n=0}^{[(N-1)/2]} H_{1+2(n+k)}(\alpha x) D(2n+1,k,\alpha) \sin (2n+1)\xi$$

for all $x > 0$ and all $\xi > 0$. The standard notation

$$[(2p+1)/2] = [(2p)/2] = p \text{ for } p = 0,1,2,\cdots \tag{23}$$

has been used. Equation (22) makes it clear that a coefficient will be indeterminate if $n\xi$ is an integral multiple of $\pi/2$ for $n \leqslant N$. This explains the severe indeterminancy which results from reliance on orthogonal view directions, e.g., $\xi = \pm\pi/4$ or $\xi = 0$ and $\pi/2$.

4. Required Data

The algorithm described above will give an estimate of α_p and C_p, and therefore of $f(r,\theta)$, even if the number of data points recorded is less than the number of unknowns, namely

$$M \equiv 1 + (2N+1)(K+1) \ . \tag{24}$$

The error bounds on such an estimate must be unsatisfactory, of course, but at least are provided by the method in the form of $\|r_p\|^2_{R_{22}}$, which can be compared to $\|g\|^2_{R_{22}}$. Substantially, but not grossly, more than M data points should be employed. It is interesting to note that there is considerable freedom to choose between an increased number of projections and an increased number of data points on each projection. So long as one is satisfied that Eq. (3), truncated to $k \leqslant K$, $n \leqslant N$, gives sufficient detail as to the behavior of $f(r,\theta)$, the coefficients can be estimated from any number N_ξ of projections, provided N_ξ and N_x, the number of data points per projection, satisfy

$$N_\xi N_x > M \ . \tag{25}$$

If the range of x over which useful data can be measured is given roughly by

$$\Delta_+ > x > -\Delta_- \tag{26}$$

and the minimum separation between independent data points is δ, then N_x is bounded by

$$N_x < (\Delta_+ + \Delta_-)/\delta \tag{27}$$

and the necessary number of projections is only restricted by

$$N_\xi > (M\delta)/(\Delta_+ + \Delta_-) \ . \tag{28}$$

Note, however, that the reconstruction from only a few projections (small N_ξ) of functions with strong azimuthal dependence (large N) is possible only because each increase in N increases the highest degree, N+2K, of the polynomials in x which are fitted to the data $g(x,\xi)$. If too great reliance is placed on this fact, since uncorrelated noise simulates the appearance of a polynomial of high degree, the values estimated for $B(n,k,\alpha)$, $D(n,k,\alpha)$ with large n will be determined primarily by the error processes, not by true data. However, one can reduce N_ξ far below the value required for numerical integration over ξ.

5. Example

Olsen, et al. [6] demonstrated their method using simulated data computed analytically to represent $g(x,\xi)$ when $f(r,\theta)$ is given by the displaced Gaussian

$$f(r,\theta) = f_0 \exp\{-\beta^2[r^2 + d^2 - 2dr\cos(\theta - \tfrac{\pi}{4})]\} \ . \tag{29}$$

AD-A074 340 ROCKWELL INTERNATIONAL THOUSAND OAKS CA SCIENCE CENTER F/G 13/8
FUNDAMENTALS OF PLASMA ARC WELDING.(U)
AUG 79 C B SHAW
UNCLASSIFIED SC5031.8FR N00014-75-C-0789
NL

2 OF 2
AD
A074340

END
DATE
FILMED
10-79
DDC

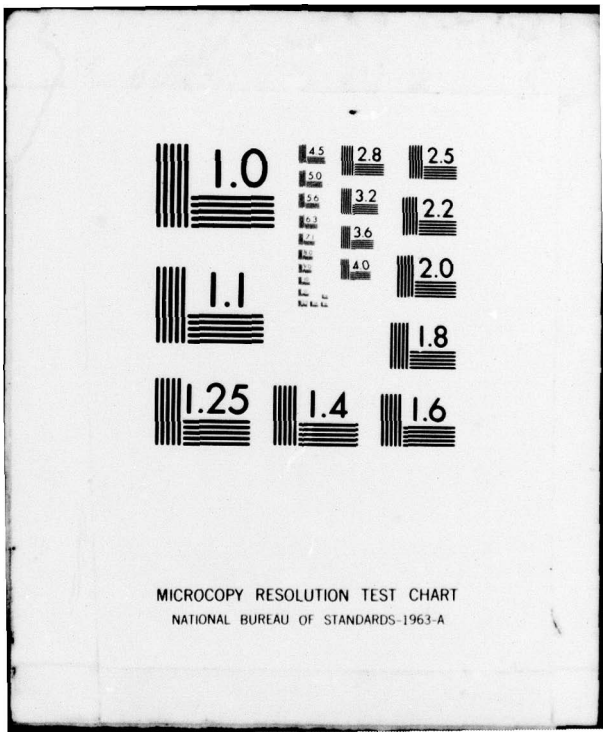
1.0
1.1
1.25
1.4
1.6
1.8
2.0
2.2
2.5
2.8
3.2
3.6
4.0
4.5
5.0
5.6
6.3
7.1
MICROCOPY RESOLUTION TEST CHART
NATIONAL BUREAU OF STANDARDS-1963-A

Use of Eqs. (1,2) gives the exact expression for $g(x,\xi)$,

$$g(x,\xi) = (f_0/\beta)\pi^{\frac{1}{2}} \exp\{-\beta^2[x - d\cos(\xi - \tfrac{\pi}{4})]^2\} . \qquad (30)$$

To express this in the form of Eq. (4), let

$$\alpha = \beta \qquad (31)$$

and verify that both Eq. (3) and Eq. (4) are satisfied by

$$B(n,k,\alpha) = A(n,k,\alpha)\cos\frac{n\pi}{4}$$

$$D(n,k,\alpha) = A(n,k,\alpha)\sin\frac{n\pi}{4} \qquad (32)$$

with

$$A(n,k,\alpha) = \frac{f_0(2-\delta_{n0})\pi^{\frac{1}{2}}(\alpha d/2)^{n+2k}}{\alpha(k!)(k+n)!} \qquad (33)$$

In Olsen, et al. [6], $g(x,\xi)$ was evaluated from Eq. (30) with $\beta = 4.13030$, $f_0 = 2.3303$, and $d = 0.1$, for ξ from 0° to 180° in 5° increments, and for x from -1 to +1 in increments of 0.0125. Numerical integration over x and ξ, using the orthoganality conditions of Eqs. (5,6), gave numerical values for the $B(n,k,\alpha)$ and $D(n,k,\alpha)$, with α assumed known and equal to β, for $0 \leq n \leq 5$ and $0 \leq k \leq 5$. That is, 5957 data points, simulated analytically, yielded values

for 66 coefficients, the scale factor having been found by knowing the exact answer in advance. Then $f(r,\theta)$ was calculated at 43 points, using Eq. (3) truncated at $n = k = 5$, and the values of α and the 66 coefficients. When comparison was made with analytical values taken from Eq. (39), the rms absolute error was 4×10^{-4} but the rms relative error was 15.9%. Table I shows the error in the distribution when reconstructed by the method presented here. The absolute rms error is worse, but relative rms error better than Olsen, in all cases. The value of α was found equal to β, to the number of decimal places defined, for P (the number of iterations on α) generally no more than 10. Note that instead of 5957 data points (161 on each of 37 projections) we could use a total of only 160, 80, or even 40 data points taken from a single pair of projections. Further, the results remained quite stable when random background and measurement errors were simulated at the indicated (equal) levels.

6. Acknowledgements

The author is deeply grateful to Harry Olsen, who generously supplied reprints and enthusiastic encouragement; to Bob Berggren for valuable programming and analytical support; to Dick Gordon for thought-provoking discussions; and to Burt Davis and Dennis Trover for invaluable help in generating the plasma diagnostic data which has been analyzed by the new algorithm as proof of its utility in

TABLE I. ERROR IN RECONSTRUCTION OF DISPLACED GAUSSIAN

Simulated Experimental Error, %	40 Data Points (10 pairs, 2 planes)		80 Data Points (20 pairs, 2 planes)		160 Data Points (40 pairs, 2 planes)	
	abs rms	rel rms	abs rms	rel rms	abs rms	rel rms
0	.0132	2.17	.0140	2.52	.0149	2.84
1	.0148	2.23	.0148	2.66	.0191	4.01
3	.0326	5.19	.0184	3.22	.0154	2.20

actual practice. The work was supported in part by Rockwell International under its Independent Research and Development Program, and in part by the United States Navy Office of Naval Research, Project 471, under Contract N00014-75-C-0789. A preliminary report was presented at the Brookhaven Workshop [5, p. 70].

REFERENCES

[1] Joel N. Franklin, Well Posed Stochastic Extensions of Ill Posed Linear Problems, J. Math. Anal. Appl. 31 (1970) 682-716.

[2] R.G. Gordon, ed., Image Processing for 2-D and 3-D Reconstruction from Projections: Theory and Practice in Medicine and the Physical Sciences, Technical Digest of Topical Meeting 4-7 August 1975, Stanford University (1975).

[3] C.D. Maldonado, Note on Orthogonal Polynomials Which Are "Invariant in Form" to Rotation of Axes, J. Math. Phys. 6 (1965) 1935-1938.

[4] C.D. Maldonado and H.N. Olsen, New Method for Obtaining Emission Coefficients from Emitted Spectral Intensities. Part II — Asymmetrical Sources. J. Opt. Soc. Am. 56 (1966) 1305-1313.

[5] R.B. Marr, ed., Techniques of Three-Dimensional Reconstruction, Proc. Int'l. Workshop 16-19 July 1974, Brookhaven National Laboratory Report BNL 20425 (1974).

[6] H.N. Olsen, C.D. Maldonado, and G.D. Duckworth, A Numerical Method for Obtaining Internal Emission Coefficients from Externally Measured Spectral Intensities of Asymmetrical Plasmas, J. Quant. Spectrosc. Radiat. Transfer 8 (1968) 1419-1430.

[7] C.B. Shaw, Jr., Improvement of the Resolution of an Instrument by Numerical Solution of an Integral Equation, J. Math. Anal. Appl. 37 (1972) 83-112.

[8] C.B. Shaw, Jr., Best Accessible Estimation: Convergence Properties and Limiting Forms of the Direct and Reduced Versions, J. Math. Anal. Appl. 44 (1973) 531-552.

[9] C.B. Shaw, Jr., B.I. Davis, and D.W. Trover, Fundamentals of Plasma Arc Welding, Annual Report No. 1, Contract No. N00014-75-C-0789, Rockwell International Science Center Document SC5031.7AR (1976).

[10] Gabor Szegö, Orthogonal Polynomials, Colloquium Publications Vol. XXIII, American Mathematical Society, Providence, Rhode Island, Ch. V (1939).